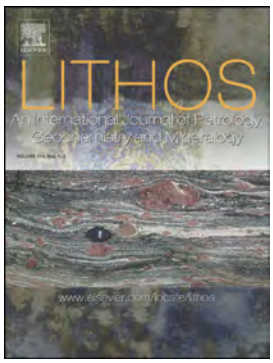

Isotopic constraints on contamination processes in the Tonian Goiás Stratiform Complex

Tommaso Giovanardi, Maurizio Mazzucchelli, Federico Lugli, Vicente A.V. Girardi, Ciro T. Correia, Colombo C.G. Tassinari, Anna Cipriani

PII: S0024-4937(18)30129-4
DOI: doi:10.1016/j.lithos.2018.04.008
Reference: LITHOS 4624

To appear in:

Received date: 5 December 2017
Accepted date: 12 April 2018

Please cite this article as: Tommaso Giovanardi, Maurizio Mazzucchelli, Federico Lugli, Vicente A.V. Girardi, Ciro T. Correia, Colombo C.G. Tassinari, Anna Cipriani , Isotopic constraints on contamination processes in the Tonian Goiás Stratiform Complex. The address for the corresponding author was captured as affiliation for all authors. Please check if appropriate. Lithos(2018), doi:10.1016/j.lithos.2018.04.008

Isotopic constraints on contamination processes in the Tonian Goiás Stratiform Complex

Tommaso Giovanardi[1,2], Maurizio Mazzucchelli[2], Federico Lugli[2], Vicente A.V. Girardi[1], Ciro T. Correia[1], Colombo C.G. Tassinari[1], Anna Cipriani[2,3].

1 Instituto de Geociências, Universidade de São Paulo, Rua do Lago 562, Cidade Universitária, B-05508-900, São Paulo, Brasil; c.a.: maurizio.mazzucchelli@unimore.it

2 Dipartimento di Scienze Chimiche e Geologiche, Università di Modena e Reggio Emilia, Via Campi 103, I-41125 Modena, Italy;

3 Lamont Doherty Earth Observatory of Columbia University, Palisades, New York, 10964, USA.

Abstract

The Tonian Goiás Stratiform Complex (TGSC, Goiás, central Brazil), is one of the largest mafic-ultramafic layered complexes in the world, emplaced during the geotectonic events that led to the Gondwana accretion. In this study, we present trace elements and in-situ U/Pb - Lu-Hf analyses of zircons and $^{87}Sr/^{86}Sr$ ratios of plagioclases from anorthosites and gabbros of the TGSC.

Although formed by three isolated bodies (Cana Brava, Niquelândia and Barro Alto), and characterized by a Lower and an Upper Sequence (LS and US), our new U/Pb zircon data confirm recent geochemical, geochronological, and structural evidences that the TGSC has originated from a single intrusive body in the Neoproterozoic.

New Hf and Sr isotope ratios construe a complex contamination history for the TGSC, with different geochemical signatures in the two sequences. The low Hf and high Sr isotope ratios of the Lower Sequence (εHf(t) from -4.2 down to -27.5; $^{87}Sr/^{86}Sr$ = 0.706605-0.729226), suggest the presence of a crustal component and are consistent with contamination from meta-pelitic and calc-silicate rocks found as xenoliths within the Sequence. The more radiogenic Hf isotope ratios and low Sr isotope composition of the Upper Sequence (εHf(t) from 11.3 down to -8.4; $^{87}Sr/^{86}Sr$ = 0.702368-0.702452), suggest a contamination from mantle-derived metabasalts in agreement with

the occurrences of amphibolite xenoliths in the US stratigraphy. The differential contamination of the two sequences is explained by the intrusion of the TGSC in a stratified crust dominated by metasedimentary rocks in its deeper part and metavolcanics at shallower levels. Moreover, the differential thermal gradient in the two crystallizing sequences might have contributed to the preservation and recrystallization of inherited zircon grains in the US and total dissolution or magmatic overgrowth of the LS zircons via melt/rock reactions processes.

Graphical abstract

Keywords

layered complex; contamination, Lu-Hf; zircon; Goias

Introduction

The Tonian Goiás Stratiform Complex (TGSC hereafter) is a large intrusion discontinuously outcropping for about 350 km along a NNE trend within the Brasilia Belt (northern Goiás, central Brasil; Giovanardi et al., 2017a, b). The TGSC model of formation has been debated for decades, mostly because of the complex geological history and stratigraphy of this intrusion that consists of three separated layered mafic-ultramafic bodies intruded into a metavolcanic-metasedimentary sequence. The three fragments are known as Barro Alto, Niquelândia and Cana Brava and characterized by a lower and an upper unit with distinct lithology. The Lower Sequence (LS) comprises ultramafics and gabbros (Correia et al., 1997, 2012; Rivalenti et al., 2008; Giovanardi et al., 2017a), whereas the Upper Sequence (US) consists of anorthosites and minor olivine-gabbros (Rivalenti et al., 2008; Correia et al., 2012).

In the two-intrusions model of formation of the TGSC, the LS and US are two separate intrusions of Neoproterozoic and Mesoproterozoic age, respectively (Pimentel et al., 2004, 2006; Ferreira Filho et al., 2010; Della Giustina et al., 2011). In the one-intrusion model, now widely accepted, the complex is a single Neoproterozoic (~790Ma) intrusive body, where the US crystallized from an

anorthositic crystal mush segregated from the precipitation of the LS ultramafics (Rivalenti et al., 2008; Correia et al., 2012; Giovanardi et al., 2017a, b).

Still debated is the role played by the metavolcanic-metasedimentary sequence during the emplacement and crystallization of the complex at crustal levels. In fact, the Sr and Nd isotope composition of LS whole rocks shows a general increase of crustal contamination across the LS moving upwards. Maximum crustal contamination is reached at the top of the sequence where dispersed xenoliths from the metavolcanic-metasedimentary country-rocks are common ($^{87}Sr/^{86}Sr_{(t)}$ from 0.706605 up to 0.736590; $\varepsilon Nd_{(t)}$ from 1.7 down to -8.5; Girardi and Kurat, 1982; Girardi et al., 1981, 1986; Correia et al., 1997, 2012; Giovanardi et al., 2017a). Conversely, whole rock Sr and Nd isotope ratios in the US are within mantle values and have led to the idea that this sequence is not contaminated by the country-rocks ($^{87}Sr/^{86}Sr_{(t)}$ from 0.702034 to 0.704293; $\varepsilon Nd_{(t)}$ from 8.0 to 4.9; Rivalenti et al., 2008; Correia et al., 2012). However, dispersed xenoliths and inherited zircons from the metavolcanic-metasedimentary sequence have been recognized throughout the US. These xenoliths are mostly amphibolites and the protoliths have been genetically related to MORB magmatism (Moraes et al., 2003, 2006).

Due to the immobile nature of the Lu-Hf isotope systematic, we carried out Lu-Hf isotopic analyses of zircon grains in gabbros and anorthosites from the LS and US sequences to unravel the complex intrusive growth and contamination history of the TGSC. In a number of samples, we also carried out U-Pb and trace elements analyses to evaluate chemical variations between inherited and magmatic zircon grains and to expand the U-Pb dataset on poorly evaluated samples previously dated by Correia et al. (2007).

Geological setting

The Tonian Goiás Stratiform Complex (TGSC) (Fig. 1) is part of the Goiás Massif (Goiás state, central Brasil). This is an exotic terrane, or microcontinent, disrupted and accreted to the São Francisco craton during the Neoproterozoic Brasiliano/Panafrican event that led to the formation of

the Gondwana supercontinent (Brito Neves and Cordani, 1991; Pimentel and Fuck, 1992; Fuck et al., 1994; Pimentel et al., 2000).

The TGSC overthrusts to the E the Rio Maranhão Thrust Zone, and, to the W, is in intrusive contact with a metavolcanic-metasedimentary sequence (Girardi and Kurat, 1982; Girardi et al., 1986; Correia and Girardi, 1998; Ferreira Filho et al., 2010). The TGSC has a typical lopolithic structure with the thicker portion of the lens corresponding to Niquelândia and the N-S trending part of Barro Alto. Towards the sides, Cana Brava to the North and Barro Alto to the East thin out.

The Lower Sequence (LS) is common to the three fragments of the TGSC, while the Upper Sequence (US) outcrops only in Niquelândia and in the N-S trending portion of Barro Alto.

The LS stratigraphy comprises the following units (Figs. 2, 3 and 4):

i) Lower Mafic Zone (LMZ). The LMZ is formed by gabbros mainly recrystallized in fine grained and mylonitic textures and/or metamorphosed in epidote-bearing amphibolites. The recrystallization is probably a consequence of the tectonic emplacement of the complexes over the Rio Maranhão Thrust Zone, with a pervasive percolation of fluids in the lower units (Girardi et al., 1986; Correia and Girardi, 1998; Correia et al., 1999; Biondi, 2014).

ii) Ultramafic Zone (UZ). The UZ is formed by variably serpentinized peridotites interlayered with amphibolites and subordinate gabbros and pyroxenites. Primary cumulus textures are commonly preserved. Upwards along the stratigraphy, the metamorphic recrystallization decreases and pyroxenites become predominant (mainly websterites and subordinate orthopyroxenites) and interlayered with gabbros. The transition to the upper unit is characterized by a decrease of pyroxenite layers and an increase of gabbros.

iii) Mafic Zone (MZ). The MZ consists of gabbros, gabbro-norites and norites and minor diorites, sometimes containing garnet. Hydrous mineral (i.e. amphibole and biotite) abundance increases discontinuously along the stratigraphy, and is maximum at the top of the unit (named by Girardi et al., 1986, as the 'Hydrous Zone' in Niquelândia). MZ rocks are commonly recrystallized under deformative conditions, from hyper- to sub-solidus, during magma emplacement and cooling and

exhibit a foliation parallel to the TGSC NNE direction. Xenoliths from the metavolcanic-metasedimentary sequence occur in decametres-long quartzite layers parallel to the TGSC foliation, and are recognized in both Niquelândia and Cana Brava. Going upwards along the stratigraphy, xenoliths become smaller, more abundant and of variable composition (e.g., amphibolites, garnet-bearing amphibolites, gneisses, metapelite and calc-silicate rocks; Correia et al., 2012; Giovanardi et al., 2017a).

The US stratigraphy is organized in the following units:

iv) Upper Gabbro-Anorthosite Zone (UGAZ). The UGAZ is formed by olivine gabbros grading into anorthosites and troctolites with local layers and lenses of subophitic coarse-grained isotropic gabbros.

v) Upper Amphibolite (UA). The US consists of amphibole-bearing gabbros interlayered with amphibolites, epidote-bearing gneisses and/or other lithologies of the country rock.

The metavolcanic-metasedimentary country rocks are named Palmeirópolis, Indaianopólis and Juscelândia sequences. Despite having different names, the three sequences have similar stratigraphy and lithologies and are therefore considered fragments of the same crustal sequence (Ferreira Filho et al. 2010 and references therein). It is formed by metasedimentary successions (i.e. metacherts, metapelites and calc-silicate rocks) with interbedded metamorphosed igneous rocks (i.e. amphibolites, gneisses and intrusive and sub-volcanic granites; Brod and Jost 1991; Araújo et al. 1995; Araújo 1996; Moraes and Fuck 1994, 1999; Moraes et al. 2003, 2006; Ferreira Filho et al. 2010). The amphibolites have MORB affinity and their basaltic protolith is interpreted as originated in a transitional setting from a continental rift to an aborted ocean basin (Araújo, 1996; Moraes et al. 2003, 2006). Geochronological data suggest a Mesoproterozoic age for the rifting event (1.26-1.30 Ga; Pimentel et al., 2000; Moraes et al., 2006; Ferreira Filho et al., 2010). The metavolcanic-metasedimentary is recrystallized in greenschist-facies in the upper portions and in amphibolite-granulite facies towards the contact with the TGSC (Moraes and Fuck, 1994; Araújo 1996; Moraes et al. 2003, 2006; Ferreira Filho et al. 2010). The age of metamorphic recrystallization is slightly

younger than the TGSC intrusion, between 767 ± 150 Ma and 745 ± 10 Ma (Sm-Nd garnet-whole rock isochron age and single-spot U-Pb zircon age; Moraes et al., 2006). However, this age range is indistinguishable within errors from the TGSC intrusion age.

Sample selection

Four samples from Cana Brava, three from Niquelândia and three from Barro Alto were selected for zircons Lu-Hf and U-Pb in situ isotope analyses. Some of these samples had already been analyzed for U-Pb isotopes by Correia et al. (2007, 2012) and Giovanardi et al. (2015, 2017b). The complete sample list, with locations and references, is reported in Table 1.

Samples from the LS of Cana Brava (named CB) are two gabbros and one diorite collected close to the upper contact with the country rock (CB1100, CB1382 and CB1030) and one gabbro from the middle of the MZ (CB1175) (Fig. 2). Sample CB1100 is a non-foliated gabbro enriched in spinel and with minor amounts of amphibole. Samples CB1382 and CB1175 are hydrous granoblastic gabbros with foliation parallel to the layer strike, marked by the alignment of amphibole, pyroxene and plagioclase. Amphibole is the most abundant hydrous phase and is commonly associated with minor biotite. K-feldspar and quartz are minor phases and apatite, spinel and zircon are accessories. Sample CB1030 is an orthopyroxene bearing diorite and contains more K-feldspar and quartz than the gabbros. Biotite is the major hydrous phase, whereas amphibole is an accessory together with apatite, titanite and zircon. Zircon grains from Cana Brava samples commonly show subhedral to euhedral habits (Giovanardi et al., 2015, 2017b).

Samples from Niquelândia (named NQ) are one gabbro from the LS (NQ1549) and two anorthosites from the US (NQ1551 and NQ1552). Sample NQ1549 is a foliated hydrous granoblastic gabbro from the top of the LS, outcropping near a large paragneiss inclusion (Fig. 3). Amphibole is the major hydrous phase, while biotite is accessory together with spinel and zircon. US samples NQ1551 and NQ1552 are anorthosites with granoblastic texture. They consist of c.a. 95 % plagioclase with minor amounts of amphibole, epidote, scapolite and zircon.

Samples from Barro Alto (named BA) are one gabbro from the LS (BA06T) and two anorthosites from the US (BA01T and BA1541, Fig. 4). LS sample BA06T is a coarse-grained layered hydrous gabbro. Layering is formed by the alternance of portions enriched in pyroxene and amphibole and portions enriched in plagioclase (Giovanardi et al., 2017b). Spinel is abundant in the mafic layers while zircon is accessory. US anorthosites BA01T and BA1541 have granoblastic textures (Correia et al., 2007). Minor amounts of clinopyroxene and amphibole occur as interstitial phases between plagioclases along deformation structures (Giovanardi et al., 2017b). Apatite, rutile, epidote and zircon are accessory phases.

Analytical methods

Zircon grains were separated after crushing, milling, magnetic and heavy liquid separation, and hand picking under a binocular microscope and embedded in resin. After Au-coating, the polished mounts were examined with a FEI-QUANTA 250 scanning electron microscope equipped with secondary-electron and cathodoluminescence (CL) detectors at the Instituto de Geociências - Centro de Pesquisas Geocronologicas - Universidade de São Paulo (IGc-CPGeo-USP); the most common conditions used in CL analysis were 60 μA of emission current, 15.0 kV of accelerating voltage, 7 μm of beam diameter, 200 μs of acquisition time, and a resolution of 2048x1887 pixels and 345 dpi. Some samples were analyzed for U-Pb isotopes using a SHRIMP-IIe also at IGc-CPGeo-USP, following the analytical procedures of Williams (1998). Correction for common Pb is based on the measured ^{204}Pb, and the typical error for the ^{206}Pb/^{238}U ratio is less than 2%; U abundance and U-Pb ratios were calibrated against the TEMORA-II standard. The dataset consists of 56 new U-Pb SHRIMP-II analyses and is reported in Supplementary Material A. Twenty-four analyses were performed on zircon grains from the US anorthosite of Barro Alto (sample BA1541) and 32 analyses were carried on zircon grains from Niquelândia, 16 for sample NQ1549 (a gabbro from the top of the LS) and 16 for sample NQ1552 (an anorthosite from US). For all samples, ^{207}Pb/^{235}U and

$^{206}Pb/^{238}U$ concordia ages (with 95% of confidence level and 2σ error) are calculated using Isoplot 4.1 software (Ludwig, 2009).

In situ Lu–Hf isotope analyses were determined at the Centro Interdipartimentale Grandi Strumenti (CIGS) of the University of Modena and Reggio Emilia (Italy) using a double focusing MC–ICP-MS with a forward Nier–Johnson geometry (Thermo Fisher Scientific, Neptune™), coupled to a 213 nm Nd:YAG laser ablation system (New Wave Research™).

During the analytical session, zircon reference materials, TEMORA-2 and CZ3, were employed to check accuracy and precision of the measurements. Eight of nine Faraday detectors were used to collect the following masses: 171Yb, 173Yb, 175Lu, 176Hf+Lu+Yb, 177Hf, 178Hf, 179Hf, 180Hf. Isotopic ratios were acquired in static mode with a block of 250 cycles (including laser warm-up, ~50–80 cycles of analysis and washout), an integration time of 0.5 s, a laser spot of 55 μm and a fluence of ~10 J/cm^2. A low laser frequency (~10 Hz) was used to achieve better signal stability (Vroon et al. 2008) with a He flux of ~0.5 L/min. Before each analysis, the surface of the zircon was pre-ablated with a spot size of 60 μm.

Data reduction was performed with the Hf-INATOR excel spreadsheet (Giovanardi & Lugli, 2017). TEMORA-2 yielded a $^{176}Hf/^{177}Hf$ ratio of 0.282689 ± 0.000080 (2σ; n = 37), identical within error to the reference value of 0.282693 (Matteini et al., 2010); similarly, CZ3 yielded a $^{176}Hf/^{177}Hf$ ratio of 0.281722 ± 0.000027 (2σ; n = 20; reference value: 0.281729; Wu et al., 2006). The complete dataset of our zircon samples consists of 145 analyses reported in Supplementary Material B. When possible, Lu-Hf analyses were carried out on the same domain of U-Pb analyses and recalculated to the $^{206}Pb/^{238}U$ single spot age. Otherwise, Lu-Hf data have been recalculated to 790 Ma, considering this age as the best representative for the complex intrusion age (see discussion; Correia et al., 2012; Giovanardi et al., 2017b). Data were calculated using the $(^{176}Hf/^{177}Hf)_{CHUR}$ and $(^{176}Lu/^{177}Hf)_{CHUR}$ present-day values of 0.282772 and 0.0332 respectively, as reported by Blichert-Toft and Albarede (1997).

On several zircon grains, already analysed by SHRIMP, U/Pb analyses were replicated at the CIGS UNIMORE by coupling the laser ablation system to a quadrupole ICP-MS X Series II (Thermo Fisher Scientific) and employing a laser spot size of 40 μm, a repetion rate of 10 Hz and a fluence of 10 J/cm^2. The ICP-MS was tuned using NIST612 glass reference material to optimize the signal intensity and stability, checking ^{139}La, ^{238}U and the ^{238}U/^{232}Th ratio. The oxide production within the plasma was monitored through the ^{232}Th^{16}O/^{232}Th ratio, constantly kept below 0.01%. Acquired masses were 202Hg, 204Pb (+204Hg), 206Pb, 207Pb, 208Pb, 232Th, 235U and 238U. ^{206}Pb/^{207}Pb, ^{207}Pb/^{235}U and ^{206}Pb/^{238}U ratios were calculated during analysis. ^{204}Pb/^{206}Pb ratio was monitored but has been always below detection limits. TEMORA-2 and CZ3 were used as known and unknown (respectively) zircon reference materials and bracketed during analysis. U-Pb ratios were thus corrected for laser induced elemental fractionation using TEMORA-2 as reference material. The complete dataset of the in situ U-Pb analyses is reported in Supplementary Material A.

Trace element analysis was performed at the CIGS UNIMORE using the same instrumental conditions presented for U-Pb determination (e.g. Lugli et al., 2017a; Sforna and Lugli, 2017). The system is equipped with a collision-reaction cell to drastically attenuate polyatomic interferences. Si, Ti, REE and Hf were acquired during two analytical sessions. Elemental quantification was performed using NIST 610, 612 and 614 as reference materials and Si, measured by electron microprobe (see methodology in Ponce et al. 2015), as internal standard. Resulting RSD for all trace element data is always better than 10%. Data are reported in Supplementary Material C.

Strontium isotopes were analysed on plagioclase separates from 2 samples (Table 2). Plagioclases were leached and dissolved, and Sr was separated using standard techniques. The ^{87}Sr/^{86}Sr ratios were measured on 200 ppb solutions by MC-ICP-MS on a Thermo Scientific Neptune housed at the CIGS UNIMORE. Samples and standards were analysed in a static multi-collection mode in single blocks of 100 cycles with an integration time of 8 seconds per cycle. The ^{87}Sr/^{86}Sr ratios were normalized to an ^{86}Sr/^{88}Sr ratio of 0.1194 and corrected for machine bias to an accepted value of

0.710260 for the NBS-987 Sr standard. Repeated analyses of the NBS-987 yielded a mean $^{87}Sr/^{86}Sr$ ratio of 0.710270 ± 0.000010 (2σ; n = 4).

In situ Sr isotope analyses (Table 2) were performed at the CIGS UNIMORE using the 213 nm laser ablation system coupled to the Neptune MC-ICP-MS (Lugli et al., 2017b). Laser ablation parameters are those for Hf isotope analyses. We collected the same sequence of masses as in the solution analyses as well as masses 85.5 and 86.5 to check doubly charged Yb interferences. Background Kr was corrected measuring 60 s of gas blank with the laser off. After background subtraction, the remaining signal on mass 82 was used to check the formation of Ca dimers and argides. Rb was corrected by calculating the ^{87}Rb contribution to mass 87 by measuring the interference-free 85Rb signal, correcting for instrumental mass fractionation, and using the natural $^{87}Rb/^{85}Rb$ ratio. The instrument was tuned for maximum sensitivity on mass 88, but also checking the accuracy of the $^{87}Sr/^{86}Sr$ ratio of an in-house reference material (modern marine shell), which yielded a Sr isotopic ratio of 0.709166 ± 0.000039 (2σ; n = 4), in agreement with modern seawater (0.70917). Repeated analyses of the international reference material JCt-1 yielded a $^{87}Sr/^{86}Sr$ ratio of 0.709151 ± 0.000013 (2σ; n = 4).

Results

Plagioclase Sr isotopes

Plagioclases from gabbro BA06T (LS) and anorthosites BA01T (US) and BA02T (US) contain on average 164 (± 8, n=30), 151 (±8, n=30) and 148 (±9, n=30) ppm of Sr, respectively. The Rb average concentration is 0.5 ± 0.4 ppm in sample BA06T, 0.2 ± 0.1 ppm in sample BA01T and 0.3 ± 0.4 ppm in BA02T, with Rb/Sr ratios of 0.0030, 0.0011 and 0.0020, respectively.

LS BA06T and US BA02T plagioclases have been analysed in situ and in solution and the results agree well with each other. The in situ $^{87}Sr/^{86}Sr$ ratio of LS BA06T is 0.729948 ± 0.000125 (2σ; n=3) and the solution is 0.729226 ± 0.000012. The in situ $^{87}Sr/^{86}Sr$ of US BA02T is 0.702444 ± 0.000329 (2σ; n=3) and the solution is 0.702368 ± 0.000012. US BA01T plagioclases were not

analysed in solution, but the in situ $^{87}Sr/^{86}Sr$ is 0.702452 ± 0.000040 (2σ; n=2), in agreement with BA02T plagioclase. Sr isotope ratios recalculated to the age of the TGSC intrusion at 790 Ma are 0.729192 and 0.729914 (in solution and in situ, respectively) for LS gabbro BA06T, 0.702355 and 0.702432 (in solution and in situ, respectively) for US anorthosite BA02T and 0.702430 (in situ) for US anorthosite BA01T (Fig. 5).

New zircon Cathodoluminescence and U-Pb geochronology

CL structures indicate the presence of magmatic and inherited zircons in the LS and US. These two populations are easily identified in gabbros from the LS, where magmatic zircon grains have well-developed linear oscillatory zoning and domains with locally bright rim reabsorbing the oscillatory zoning (Fig. 6A; Correia et al., 2007; Giovanardi et al., 2015, 2017b). Rare anhedral zircon grains commonly show irregular chaotic zoning and reabsorption domains, and are interpreted as inherited, together with rare chaotic and partially reabsorbed cores (Fig. 6B; Giovanardi et al., 2015, 2017b). The distinction in magmatic and inherited zircons in the US is more complicated, mostly because zircon grains are rare in anorthosite and are common only in anorthosites containing orthopyroxene and oxides (Scoates and Chamberlain, 1995; Ashwal, 2013; Mohan et al., 2013). Anorthosite zircon grains commonly show weak or no CL structures, similar to zircon grains found in other anorthosite complexes worldwide (e.g. the Fiskænesset complex, the Duluth complex, the Sittampundi complex, and others; Polat et al., 2010; Schmitz et al., 2003; Mohan et al., 2013). However, a number of small characteristics have been identified and US zircon grains have been divided in three main groups. “Group 1” consists of anhedral to subhedral extremely fractured zircon grains, which in CL images show almost homogeneous emission (Fig. 6C). “Group 2” comprises anhedral to sub-euhedral zircon grains with poor zonations, but distinct bright and dark cores and rims (Fig. 6D). “Group 3” includes clearly magmatic fragments of crystals with linear zoning and domains (Fig. 6E), but were recognized only in the US anorthosite NQ1551 of Niquelandia previously dated by Correia et al. (2012).

Barro Alto US anorthosite (sample BA1541)

Based on CL features, zircon grains are anhedral to sub-euhedral, sometimes fractured, and belong to "Group 1" and "Group 2" (Fig 6).

Twenty-four U-Pb SHRIMP analyses on 23 zircon grains from both groups yielded 21 concordant ages ranging from 863 ± 33 Ma to 731 ± 54 Ma ($^{206}Pb/^{238}U$ single spot age, 2SE error), with a weighted average of 774 ± 12 Ma (95% confidence error level, MSWD = 2.2; Fig. 7) and a concordia age of 780 ± 10 Ma (95% confidence error level, decay-const. errs included, MSWD = 0.48, probability of concordance = 0.49; Fig. 7). Two discordant ages were discarded, but fall within this range. Two older concordant $^{206}Pb/^{238}U$ single spot age of 1034 ± 19 Ma and 944 ±224 Ma were also obtained, one in each group of zircon grains.

Niquelândia LS gabbro (sample NQ1549)

Zircon grains are generally magmatic, euhedral to subhedral and commonly show an oscillatory magmatic zonation in CL (Fig. 8). This zonation is locally truncated by a discordant, thin bright rim (Fig. 8). Few zircon grains are characterized by an inherited core commonly bright and unzoned in CL (Fig. 8).

Sixteen analyses were performed on 7 zircon grains. Eleven analyses yielded concordant ages ranging from 793 ± 22 Ma to 759 ± 22 Ma ($^{206}Pb/^{238}U$ single spot age, 2SE error), with a weighted average of 771 ± 8 Ma (95% confidence error level, MSWD = 1.5; Fig. 8) and a concordia age of 772 ± 6 Ma (95% confidence error level, decay-const. errs included, MSWD = 2.8, probability of concordance = 0.09; Fig. 8). A younger discordant analysis gave a $^{206}Pb/^{238}U$ single spot age at 756 ± 35 Ma. Four concordant analyses from inherited cores provide older $^{206}Pb/^{238}U$ ages, between 1364 ± 54 Ma and 1063 ± 45 Ma.

Niquelândia US anorthosite (sample NQ1552)

Zircon grains are anhedral to subhedral and commonly fractured and based on CL images pertain to "Group 1" (Fig. 9). In addition, some zircons grains in CL image were characterized by unzoned, extremely bright crystals and did not provide good quality analyses (Fig. 9).

Fifteen analyses from yielded concordant ages ranging from 975 ± 37 Ma to 762 ± 24 Ma ($^{206}Pb/^{238}U$ single spot age, 2SE error; Fig. 9). One discordant age at 880 Ma falls in the interval.

Lu-Hf zircon data

A total of one-hundred and forty-five Hf isotope ratios were obtained in situ on zircon grains and the age corrected epsilon Hf are plotted in Figure 9 with their respective U/Pb ages.

LS magmatic zircon grains have εHf(t) ranging between -25.1 and -4.8 in Cana Brava (gabbros and diorite), between -15.8 and -8.3 in Barro Alto (gabbro BA06T) and between -27.6 and 5.9 in Niquelândia (gabbro NQ1549).

The US Barro Alto anorthosite zircons ("Group 1" and "Group 2") range from -16.1 to 11.3, with the US anorthosite sample BA1541 falling within a smaller εHf(t) range, between -3.6 and 2.4 (Fig. 10). Niquelândia US anorthosite zircon grains plot between -3.0 and 4.6 (Sample NQ1552, "Group 1") and between 5.3 and 7.7 (Sample NQ1551, "Group 3") with one value down to εHf(t) -7.7. Mesoproterozoic cores of US Niquelândia show positive values (εHf(t) = 2.0 and 5.9), commonly higher compared to rims.

Overall, the LS gabbros from the three complexes are characterized by the same εHf(t) range, with sub-chondritic values (Fig. 10). Similarly, zircon grains from the US samples mostly overlap in terms of εHf(t), but, with few exceptions, the εHf(t) values of US zircon grains are less negative than those of the LS (Fig. 10).

The few LS inherited zircon grains have generally lower εHf(t) values than US inherited zircons (εHf(t) on average of -6.8 vs. +2.6 respectively).

With the exception of a few radiogenic values, US zircon grains form a decreasing εHf(t) linear trend from older zircon grains to younger ones (Fig. 10): the εHf(t) values range from positive

(older zircons) to slightly negative (younger zircons). However, given the low Lu/Hf ratio of zircons this trend is controlled by the different age used to recalculate the εHf(t) values.

Zircon trace elements

Magmatic and inherited zircon grains of the LS have overlapping REE patterns with a larger variation of LREE compared to HREE and pronounced Ce positive and Eu negative anomalies (Fig. 11).

The only clear group of US magmatic zircons, zircon grains of "Group 3" from Niquelandia US anorthosite NQ1551, display a very peculiar REE pattern with a pronounced Ce anomaly, but small or no negative Eu anomaly (Fig. 11; $(Eu/Eu^*)_N$ between 0.8 and 1.0). Two similar patterns have been recognized in inherited zircon grains in the US of Niquelandia and Barro Alto (reported in grey in Fig. 11, with $(Eu/Eu^*)_N$ between 0.9 and 1.3).

"Group 1" and "Group 2" US zircon grains have REE patterns similar to LS zircon grains, but commonly show slightly lower REE abundances (e.g., Lu between 10 and 55 ppm and between 20 and 143 ppm, respectively) and less pronounced Eu negative anomalies (Fig. 11).

Three zircon grains from US Barro Alto and US Niquelandia show flat LREE trends with small or no Ce anomaly (Fig. 11). Similar REE patterns have been recognized in hydrothermal zircons (Hoskin and Schaltegger, 2003; Yang et al., 2014).

Overall, an increase in the La content is accompanied by an increase in REE abundances in both LS and US zircon grains.

Discussion

The TGSC geochronology revisited

Our new U/Pb zircon data, together with previous results, strongly support the one-intrusion model of formation of the TGSC, where the LS and the US originated during the same intrusive event in the Neoproterozoic (Giovanardi et al 2017b). In fact, all U/Pb ages taken together exhibit a

preponderant peak of concordant ages at ca. 790 (Fig. 12; Pimentel et al., 2004; Correia et al., 2007, 2012; Ferreira Filho et al., 2010; Della Giustina et al., 2011; Giovanardi et al., 2015, 2017b). Ages from LS linear zoning domains form a dominant peak between 770 Ma and 800 Ma, whereas ages from LS inherited cores are commonly discordant and range from Neoproterozoic up to 1957 Ma (SHRIMP analysis, Pimentel et al., 2004). Ages of the US range from Neoproterozoic up to 2052 Ma (SHRIMP analysis, Giovanardi et al., 2017b) with the maximum peak of concordant ages at ca. 790 Ma, undistinguishable, within errors, from the LS (Fig. 12). Ages older than 825 Ma, in inherited zircons, are discordant suggesting a partial reset of the U-Pb zircon system possibly during residence in the crystal mush. As far as U/Pb ages of the samples used in this study, "Group 1" zircon grains tend to provide dispersed discordant ages, "Group 2" zircons yielded concordant Neoproterozoic ages in zoned sectors and discordant older ages in unzoned sectors, and "Group 3" consists of commonly concordant Neoproterozoic ages (Correia et al., 2012; Giovanardi et al., 2017b). These age differences confirm that "Group 3" zircons are magmatic, while "Group 1" and "Group 2" are inherited with different degrees of U-Pb system resetting. However, because some Neoproterozoic ages have been obtained from "Group 2", we cannot exclude that some of these zircon grains are magmatic.

Ages younger than 770 Ma could reflect a continuous deformation-recrystallization during the cooling of the TGSC. A model of growth via multiple pulses in a deformative-active geodynamic setting has been previously proposed, with recrystallization of the TGSC under deformative conditions creating a super-imposed foliation. This foliation has been frequently interpreted as related to a regional metamorphic event younger than the TGSC intrusion event (Pimentel et al., 2004; Ferreira Filho et al., 2010; Della Giustina et al., 2011 and references therein). However, more recent studies have demonstrated that the deformation was sin-magmatic, showing features similar to other mafic complexes worldwide and in particular to the central Ivrea-Verbano mafic complex (Italy; Correia et al., 2012; Giovanardi et al., 2017a). A long lasting thermal perturbation has taken place in the Ivrea-Verbano complex with igneous activity beginning with sporadic pulses at

approximately 314 Ma (represented by small bodies as Monte Capio or Albo sills or the "appinites" dykes and sills; Kotzli et al., 2014 and references therein) and with the main igneous activity lasting for about 10 Ma (from ca. 289 to ca. 280 Ma, Quick et al., 2009). Younger ages in the Ivrea-Verbano Mafic Complex, recognized only in zircons from the lower part of the complex, have been related to the slow cooling of the intrusion from 285 to ca. 273 Ma during continuous deformation-recrystallization/cooling in the deepest levels of the complex (Sinigoi et al., 2011). A similar process might explain the few younger ages from zircon grains in the LS, the deepest portion of the TGSC complex.

Inherited zircons from the country rocks

By means of zircon age distribution and CL images, we have been able to identify several inherited zircons in the US and LS (Fig. 12), which also differ in their trace element and isotopic signatures (Fig.s 10 and 11). LS inherited zircon grains have higher REE abundances, larger Eu negative anomalies and lower εHf(t) values than US inherited zircons (εHf(t) averages of -6.8 vs. +2.6 respectively). These data are in agreement with the occurrence of country rock xenoliths in the two sequences. In fact, xenoliths in the LS are quartzites (near the base of the MZ), meta-pelite, calc-silicate rocks and subordinate amphibolites (Girardi et al., 1981, 1986; Correia et al., 1997, 2012; Giovanardi et al., 2017a), whereas xenoliths in the US are mainly amphibolites with minor amounts of calc-silicate rocks near the LS-US transition (Girardi et al., 1981, 1986; Correia et al., 1997, 2012; Giovanardi et al., 2017a). The protolith of the amphibolites has been associated to MORB magmatism, which presumably occurred between 1.26 and 1.30 Ga (Pimentel et al., 2000; Moraes et al., 2006). Inherited zircon grains from the US show εHf(t) values, recalculated to the age of the MORB magmatic event (i.e. 1.3 Ga), corresponding to mantle values (between 5.5 and 13.9, on average = 9.4), with the exception of a single zircon at -16.5. On the contrary, $\varepsilon Hf_{(1300)}$ values of LS inherited zircons are comparable with continental crust values and range between -14.1 and 7.6 with an average value of -3.2. Therefore, the different $\varepsilon Hf_{(1300)}$ values in the US and LS reflect the

distinct lithology of the xenoliths occurrences in the two sequences. The dominant $\varepsilon Hf_{(1300)}$ mantle values in the US are consistent with the predominance of amphibolite xenoliths, while the negative $\varepsilon Hf_{(1300)}$ values of LS inherited zircons are in agreement with the metasedimentary nature of the LS xenoliths.

Inherited zircons are more common in the US than in the LS (Fig.s 10 and 13). The well-defined linear trend obtained for the US inherited zircon grains in Fig 9 suggests that these zircon grains experienced a re-opening of the system, which caused Pb loss and age rejuvenation during the emplacement of the sequence (Vervoort and Kemp, 2016). The εHf(t) values of inherited LS zircons show a remarkable gap between ca. 900 and ca. 1300 Ma (Fig. 13). The lower abundance of inherited zircon grains in the LS could be the result of a more efficient Pb loss process in the LS compared to the US. An alternative explanation could be related to the higher heat produced by a gabbroic melt with respect to the one produced by an anorthositic crystal mush, and, as a consequence, a more efficient reabsorption process in the LS caused by the higher T of the gabbroic melt. Moreover, the solidus temperature of a paragneiss is lower than that one of an amphibolite. Therefore, inherited zircons from amphibolites could be preferentially preserved with respect to inherited zircons from metasedimentary rocks. In addition, inherited zircons in the LS are only recognized as small rounded cores, surrounded by magmatic growth of the crystal, whereas US "Group 1" and "Group 2" zircon grains are commonly fractured and show uniform or poorly zonated sectors without evidences of different growth stages (Fig. 6). These features suggest that in the LS inherited zircon grains have been partially resorbed under high T magmatic conditions and that in the US inherited zircons have been recrystallized at lower temperature (Kunz et al., 2018 and references therein).

The magmatic affinities of the LS and US

The new Sr isotopes data from magmatic plagioclases in the TGSC highlight a strong compositional difference between the LS and US of Barro Alto, with the LS plagioclases characterized by crustal

values ($^{87}Sr/^{86}Sr_{(790)}$ of 0.7295) and the US plagioclases by mantle values ($^{87}Sr/^{86}Sr_{(790)}$ of 0.7024). Although very different from each other, these Sr isotope ratios are very similar to those found in the corresponding sequences of Niquelandia and Cana Brava. The $^{87}Sr/^{86}Sr_{(790)}$ in LS of Niquelandia and Cana Brava varies from 0.7215 to 0.7366, and in Niquelandia US is around 0.702 (Correia et al., 2012; Giovanardi et al., 2017a; Fig. 5).

For the LS rocks, the Sr isotope ratios, together with Nd isotopes from Niquelandia and Cana Brava and Lu-Hf zircon data, suggest that the LS rocks have a strong affinity with a crustal component ($\varepsilon Nd_{(790)}$ from 1.70 to -8.47 for Cana Brava and from -1.30 to -8.70 for Niquelandia; Correia et al., 2012; Giovanardi et al., 2017a). Moreover, Sr and Nd isotopic values in the LS show an increase of the crustal component along the stratigraphy (Fig. 5). This trend has been previously interpreted as indicative of a continuous contamination along the stratigraphy from the country crustal rocks (Rivalenti et al., 2008; Correia et al., 2012; Giovanardi et al., 2017a). This is consistent with the widespread occurrence of crustal xenoliths in the LS (Girardi et al., 1981, 1986; Rivalenti et al., 2008; Correia et al., 2012; Giovanardi et al., 2017a, b). Therefore, the crustal values of the LS magmatic zircon grains and plagioclases suggest they crystallized from an extremely contaminated melt, if not directly from a melt derived from the xenoliths of the country rock itself.

Conversely, the US Sr and Nd isotope ratios are compatible with mantle values ($\varepsilon Nd_{(790)}$ from 9.76 to 2.96 for Niquelandia; Giovanardi et al., 2017a; Fig. 5) and the εHf(t) of the US zircon grains varies between 11.3 and -16.1, from mantle to sub-chondritic/crustal values. However, as discussed above, most of the US zircon grains are inherited crystals partially/totally reset at the age of the TGSC intrusion and therefore should not be used to define the isotope affinity of the US. Among the magmatic US zircon grains, "Group 3" shows the highest εHf(t) between 5.3 and 7.7, together with one magmatic zircon from US anorthosite BA01T at 11.3 of εHf(t) (Fig 9). Moreover, they are characterized by small or no Eu negative anomaly ($(Eu/Eu^*)_N$ between 0.8 and 1.0), which could be possibly due to different f_{O2} conditions of the parent melt (Trail et al., 2012) or simply to zircon crystallization before plagioclase precipitation. The lower REE contents with respect to other zircon

grains support the second hypothesis. Therefore, given that Hf is not easily mobilized in zircons (Kinny and Maas, 2003), the εHf(t) values of the US magmatic zircon grains should reflect the original isotopic composition of the US parent melt, pointing towards a depleted mantle origin. However, the large presence in the US sequence of amphibolite xenoliths with MORB affinity and of radiogenic εHf(t) inherited zircons does not exclude a contamination process, but with a contaminant with similar geochemical affinity via reactive bulk assimilation (Beard et al., 2005). This model requires a small amount of heat compared to melting and anatectic melt assimilation processes (Beard et al., 2005) and is consistent with the evidence that LS inherited zircons are commonly reabsorbed whereas US inherited zircons are not.

The consistent behaviour of Sr and Nd isotopes in bulk rocks and plagioclases and the Hf isotope ratios in zircon grains suggest that isotope systematics in the TGSC reflect the composition of the melts from which the two sequences crystallized from, and were little or not affected by later events. Therefore, the old idea that the TGSC has been recrystallized by granulite- and amphibolite-facies regional metamorphic events (also with fluids occurrences, Pimentel et al., 2004, 2006; Ferreira Filho et al., 2010; Della Giustina et al., 2011) must be discarded.

Model of TGSC contamination using zircon Hf isotopes

Given that both the LS and US rocks share geochemical features similar to xenoliths assimilated during the emplacement of the TGSC, we try now to model possible evolution paths of contamination using the Hf isotope composition of inherited zircon grains as the true $^{176}Hf/^{177}Hf$ of the bulk rock contaminant.

We recalculated this value in both sequences from the $^{176}Hf/^{177}Hf_{(t)}$ of inherited zircon grains in each sequence and $^{176}Lu/^{177}Hf$ ratios from bulk rock analyses of the respective xenoliths. Given that the age of the xenoliths is still uncertain, we used the 1.3 Ga age of the MORB volcanic event documented in the metavolcanic-metasedimentary sequence. The $^{176}Hf/^{177}Hf_{(1300)}$ average of the LS bulk rock contaminant is 0.281866 and therefore of crustal affinity ($\varepsilon Hf_{(t)}$ = -3.2; Fig. 13). Instead,

the $^{176}Hf/^{177}Hf_{(1300)}$ of the US bulk rock contaminant is 0.282224 with a clear depleted mantle character ($\varepsilon Hf_{(t)}$ = 9.5; Fig. 13). We note here that the US $^{176}Hf/^{177}Hf_{(1300)}$ value has been recalculated only from inherited zircons grains older than 825 Ma. As explained earlier, the majority of the zircon grains found in the US are inherited. However, based on the fact that anorthosite zircons found in other complexes commonly show weak or no CL features (Polat et al., 2010; Schmitz et al., 2004; Mohan et al., 2013), it cannot be ruled out that some zircons from "Group 1" and "Group 2" are magmatic. Within this scenario, we have considered magmatic all the US zircon grains with concordant Neoproterozoic ages consistent with the TGSC intrusion and inherited only the zircon grains older than 825 Ma.

Evolution lines of the bulk contaminant for the US and LS are shown in Fig 12. At 790 Ma, most of the LS zircon grains fall between the $\varepsilon Hf_{(790)}$ of the bulk rock contaminant evolution trends, between -14.5 and -3.6 (Fig. 13). The least radiogenic LS magmatic zircon grains can be modelled starting from the lowest $^{176}Hf/^{177}Hf_{(1300)}$ of LS inherited zircon grains, which provides $\varepsilon Hf_{(790)}$ of the contaminants between -25.3 and -14.4. The absence of inherited domains in these magmatic zircon grains suggests their crystallization from a melt extremely contaminated by a crustal component at the time of crystallization.

At 790 Ma, the maximum and minimum evolution trends of the bulk rock contaminant for the US scenario range between 1.1 and 13.0 $\varepsilon Hf_{(790)}$ and can only explain the small portion of truly magmatic US zircon grains (Fig. 13). Neoproterozoic "Group 1" and "Group 2" zircon grains have $\varepsilon Hf_{(t)}$ from chondritic to slightly subchondritic suggesting a weak crustal contamination of the US and can be modelled only by contamination from amphibolites with lower $^{176}Hf/^{177}Hf$ and $^{176}Lu/^{177}Hf$ ratios (Fig. 13). Six US zircon grains with $\varepsilon Hf_{(t)}$ between -3.0 and -8.4 definitely require a more crustal component, which is however compatible with the rare occurrence of metasedimentary country rocks xenoliths in the US at the LS/US boundary. Alternatively, these six zircon grains can be interpreted as totally reset inherited zircon grains.

Conclusions

New trace and isotopic Lu-Hf analyses on a large set of new and previously dated zircon grains from the TGSC complex, together with new Sr isotopes from Barro Alto plagioclases, provide new evidences on the growth and contamination processes of the TGSC.

The occurrence of inherited zircon grains in both LS and US has led us to identify that the TGSC intruded a stratified crust dominated by metasedimentary rocks in its lower part and metavolcanic at shallow levels. The intrusion of the LS within the country metasedimentary sequence has resulted in a clear crustal signature (negative εHf(t) zircon values), coherent with bulk-rock Rb-Sr and Sm-Nd isotopes. The emplacement of the US at shallower crustal levels, characterized by amphibolites with MORB-mantle like signature, has resulted in zircon εHf(t) values from slightly positive to negative. We interpret the great abundance of inherited zircon grains within the US with chondritic to sub chondritic εHf(t), at the TGSC intrusion age, as the evidence for reactive bulk rock assimilation of the amphibolite country rocks. The similar original geochemical affinities of the US TGSC parent magma and amphibolite xenoliths have masked the contamination processes in the US in the Rb-Sr and Sm-Nd bulk-rock systematics. The LS and US were, thus, both contaminated during the TGSC intrusion, resulting in different geochemical affinities due to the different composition of the contaminants.

Finally, we interpret the higher abundance of inherited zircons in the US with respect to LS due to the different thermal conditions between the two sequences. Inherited zircons in the LS are mostly reabsorbed grains at the core of magmatic overgrowth, while US inherited zircons are mainly preserved as recrystallized grains, showing homogeneous CL and no evidences for different growth events.

Acknowledgements

This work was supported by FAPESP (Fundação de Amparo à Pesquisa do Estado de São Paulo) in the frame of the project 2013/19519-6 to TG. Analytical facilities and their development have been funded by the MIUR PRIN 2015 Prot. 20158A9CBM_005 to MM and Programma Giovani Ricercatori "Rita Levi Montalcini" to AC.

We thank F. Corfu and an anonymous reviewer fot their constructive comments and Dr. Marine Farmer for improving the quality of the text.

References

Anders, E., Edibara, M., 1992. Solar system abundances of the elements. Geochimica and Cosmochimica Acta 46, 2363-2380.

Araújo, S.M., Fawcett, J.J., Scott, S.D., 1995. Metamorphism of hydrothermally altered rocks in a volcanogenic massive sulfide deposit: the Palmeirópolis, brazil, example. Revista Brasileira de Geociências 25(3), 173-184.

Araújo, S.M., 1996. Geochemical and isotopic characteristics of alteration zones in highly metamorphosed volcanogenic massive sulfide deposits and their potential application to mineral exploration. Unpublished Ph.D. Thesis, Department of Geology, University of Toronto, Canada, 210.

Ashwal, L.D., 2013. Anorthosites. Springer Science & Business Media, 2013, 422.

Beard, J.S., Ragland, P.C., Crawford, M.L., 2005. Reactive bulk assimilation: A model for crust-mantle mixing in silicic magmas. Geology 33, 681-684.

Belusova, E.A., Griffin, W.L., O'Reilly, S.Y., Fisher, N.I., 2002. Igneous zircon: trace element composition as an indicator of source rock type. Contributions to Mineralogy and Petrology 143, 602-622.

Biondi, J.C., 2014. Neoproterozoic Cana Brava chrysotile deposit (Goiás, Brazil): Geology and geochemistry of chrysotile vein formation. Lithos 184-187, 132-154.

Blichert-Toft, F., Albarede, F., 1997. The Lu–Hf isotope geochemistry of chondrites and the evolution of the mantle–crust system. Earth and Planetary Science Letters 148, 243–258.

Blichert-Toft, F., Albarede, F., Gleason, J.D., Kring, D.A., Hill, D.H., Boynton, W.V., 1998. Lu-Hf isotopic compositions of SNC meteorites: Implications for Martian mantle evolution. Goldschmidt conference abstract, in Mineralogical Magazine 62A.

Brito Neves, B.B., Cordani, U.G., 1991. Tectonic evolution of South America during the late Proterozoic. Precambrian Research 53, 23–40.

Brod, J.A., Jost, H., 1991. Características estruturais, litológicas e magmáticas da zona de cisalhamento dúctil do Rio Traíras, bloco do Complexo Niquelândia, Goiás. Revista Brasileira de Geociências 21, 205-217.

Correia, C.T., Girardi, V.A.V., 1998. Geoquimica e petrologia das rochas maficas e ultramaficas do complexo estratiforme de Cana Brava - GO, e das suas encaixantes. Boletim de Instituto de Geociências USP 29, 1-37.

Correia, C.T., Girardi, V.A.V., Tassinari, C.G., Jost, H., 1997. Rb-Sr and Sm-Nd geochronology of the Cana Brava layered mafic-ultramafic intrusion, Brasil, and considerations regarding its tectonic evolution. Revista Brasileira de Geociências 27(2), 163-168.

Correia, C.T., Jost, H., Tassinari, C.C.G., Girardi, V.A.V., Kinny, P.D., 1999. Ectasian Mesoproterozoic U–Pb ages (SHRIMP II) for themetavolcano-sedimentary sequences of Juscelandia and Indaianopolis and for the high grade metamorphosed rocks of the Barro Alto stratiform igneous complex, Goiàs State, Central Brasil. II° South Am Symp Isotopic Geology, Cordoba, Argentina, Actas, 31-33.

Correia, C.T., Girardi, V.A.V., Basei, M.A.S., Nutman, A., 2007. Cryogenian U–Pb (Shrimp I) zircon ages of anorthosites from the US of Niquelandia and Barro Alto Complexes, Central Brasil. Revista Brasileira de Geociências 37, 70-75.

Correia, C.T., Sinigoi, S., Girardi, V.A.V., Mazzucchelli, M., Tassinari, C.C.G., Giovanardi, T., 2012. The growth of large mafic intrusions: Comparing Niquelandia and Ivrea igneous complexes. Lithos 155, 167-182.

Della Giustina, M.E.S., Pimentel, M.M., Ferreira Filho, C.F., Fuck, R.A., Andrade, S., 2011. U–Pb–Hf-trace element systematics and geochronology of zircon from a granulite-facies metamorphosed mafic–ultramafic layered complex in Central Brazil. Precambrian Research 189, 172-192.

Ferreira Filho, C.S., Pimentel, M.M., Maria de Araujo, S., Laux, J.H., 2010. Layered intrusions and volcanic sequences in Central Brazil: geological and geochronological constraints for Mesoproterozoic (1.25 Ga) and Neoproterozoic (0.79 Ga) igneous associations. Precambrian Research 183, 617-634.

Fuck, R.A., Pimentel, M.M., Silva, L.J.H.D., 1994. Compartimentação tectônica da porção oriental da Província Tocantins. In: 38th Cong. Bras. Geologia, vol. 1 , 215–216.

Giovanardi, T., Lugli, F., 2017. The Hf-INATOR: A free data reduction spreadsheet for Lu/Hf isotope analysis. Earth Science Informatics 10, 517-523.

Giovanardi, T., Girardi, V.A.V., Correia, C.T., Sinigoi, S., Tassinari, C.C.G., Mazzucchelli, M., 2015. U-Pb zircons SHRIMP data from the Cana Brava Layered Complex: New constraints for the mafic-ultramafic intrusions of Northern Goiás, Brazil. Open Geosciences7, 197-206.

Giovanardi, T., Girardi, V.A.V., Correia, C.T., Sinigoi, S., Tassinari, C.C.G., Mazzucchelli, M., 2017a. The growth and contamination mechanism of the Cana Brava layered mafic-ultramafic complex: new field and geochemical evidences. Mineralogy and Petrology 111, 291-314.

Giovanardi, T., Girardi, V.A.V., Correia, C.T., Tassinari, C.C.G., Sato, K., Cipriani, A., Mazzucchelli, M., 2017b. New U–Pb SHRIMP-II zircon intrusion ages of the Cana Brava and Barro Alto layered complexes, central Brazil: Constraints on the genesis and evolution of the Tonian Goias Stratiform Complex. Lithos 282-283, 339-357.

Girardi, V.A.V., Kurat, G., 1982. Precambrian mafic and ultramafic rocks of the Cana Brava Complex, Brazil - mineral compositions and evolution. Revista Brasileira de Geociências 12(1-3), 313-323.

Girardi, V.A.V., Rivalenti, G., Sinigoi, S., 1981. Precambrian Barro Alto complex of Goias, Brazil: bulk geochemistry and phase equilibria. Neues Jahrbuch für Mineralogie Abhandlungen 142(3), 270-291.

Girardi, V.A.V., Rivalenti, G., Sinigoi, S., 1986. The petrogenesis of Niquelandia layered basic–ultrabasic complex, central Goias, Brasil. Journal of Petrology 27, 715-744.

Griffin, W.L., Pearson, N.J., Belousova, E., Jackson, S.E., van Achterbergh, E., O'Reilly, S.Y., Shee, S.R., 2000. The Hf isotope composition of cratonic mantle: LAM-MC-ICPMS analysis of zircon megacrysts in kimberlites. Geochimica et Cosmochimica Acta 64, 133–147.

Hoskin, P.W.O., Schaltegger, U., 2003. The composition of zircon and igneous and metamorphic petrogenesis. Reviews in Mineralogy and Geochemistry 53, 27-62.

Kinny, P.D., Maas, R., 2003. Lu–Hf and Sm–Nd isotope systems in zircon. In: Zircons, American Mineralogist, 327-341.

Klotzli, U.S., Sinigoi, S., Quick, J.E., Demarchi, G., Tassinari, C.C.G., Sato, K., Günes, Z., 2014. Duration of igneous activity in the Sesia Magmatic System and implications for high-temperature metamorphism in the Ivrea–Verbano deep crust. Lithos 206-207, 19-33.

Kunz, B.E., Regis, D., Engi, M., 2018. Zircon ages in granulite facies rocks: decoupling from geochemistry above 850 °C?. Contributions to Mineralogy and Petrology 173, 26. https://doi.org/10.1007/s00410-018-1454-5

Ludwig, K.R., 2009. Isoplot 4.1. A geochronological toolkit for Microsoft Excel. Berkeley Geochronology Center special publication 4, 76.

Lugli, F., Brunelli, D., Cipriani, A., Bosi, G., Traversari, M., Gruppioni, G., 2017a. C4-Plant Foraging in Northern Italy: Stable Isotopes, Sr/Ca and Ba/Ca Data of Human Osteological Samples from Roccapelago (16th–18th Centuries AD). Archaeometry 59, 1119-1134.

Lugli, F., Cipriani, A., Peretto, C., Mazzucchelli, M., Brunelli, D., 2017b. In situ high spatial resolution 87Sr/86Sr ratio determination of two Middle Pleistocene (c.a. 580 ka) *Stephanorhinus hundsheimensis* teeth by LA–MC–ICP–MS. International Journal of Mass Spectrometry 412, 38-48.

Matteini, M., Dantas, E.L., Pimentel, M.M., Bühn, B., 2010. Combined U-Pb and Lu-Hf isotope analyses by laser ablationMC-ICP-MS: methodology and applications. Anais da Academia Brasileira de Ciências 82, 479-491.

Mohan, M.R., Satyanarayanan, M., Santosh, M., Sylvester, P.J., Tubrett, M., Lam, R., 2013. Neoarchean suprasubduction zone arc magmatism in southern India: Geochemistry, zircon U-Pb geochronology and Hf isotopes of the Sittampundi Anorthosite Complex. Gondwana Research 23, 539-557.

Moraes, R., Fuck, R.A., 1994. Deformação e metamorfismo das sequências Juscelândia e Serra da Malacacheta, Complexo Barro Alto, Goiás. Revista Brasileira de Geociências 24, 189–197.

Moraes, R., Fuck, R.A., 1999. Trajetória P–T Horária para oMetamorfismo da Sequência Juscelândia, Goiás: Condições do Metamorfismo e Implicações Tectônicas. Revista Brasileira de Geociências 29, 603–612.

Moraes, R., Fuck, R.A., Pimentel, M.M., Gioia, S.M.C.L., Figueiredo, A.M.G., 2003. Geochemistry and Sm–Nd isotope characteristics of bimodal volcanic rocks of Juscelândia, Goiás, Brazil: Mesoproterozoic transition from continental rift to ocean basin. Precambrian Research 125, 317-336.

Moraes, R., Fuck, R.A., Pimentel, M.M., Gioia, S.M.C.L., Hollanda, M.H.B.M., Armstrong, R., 2006. The bimodal rift-related volcanosedimentary sequence in Central Brazil: Mesoproterozoic extension and Neoproterozoic metamorphism. Journal of South American Earth Sciences 20, 287-301.

Nowell, G.M., Kempton, P.D., Noble, S.R., Fitton, J.G., Saunders, A.D., Mahoney, J.J., Taylor, R.N., 1998. High precision Hf isotope measurements of MORB and OIB by thermal ionisation mass spectrometry: insights into the depleted mantle. Chemical Geology 149, 211–233.

Oliveira Cordeiro, P.F., Oliveira, C.G., 2017. The Goiás Massif: Implications for a pre-Columbia 2.2–2.0 Ga continent-wide amalgamation cycle in central Brazil. Precambrian Research, 298, 403-420.

Pimentel, M.M., Fuck, R.A., 1992. Neoproterozoic crustal accrction in central Brazil. Geology 20, 375-379.

Pimentel, M.M., Fuck, R.A., Jost, H., Ferreira Filho, C.F., Araujo, S.M., 2000. The basement of the Brasília Fold Belt and the Goiás Magmatic Arc. In: Cordani UG, Milani EJ, Thomaz Filho A, Campos DA (Eds.), The Tectonic Evolution of South America, Rio de Janeiro. Proceedings of the 31st International Geological Congress, Rio de Janeiro, 195-229.

Pimentel, M.M., Ferreira Filho, C.F., Amstrong, R.A., 2004. Shrimp U–Pb and Sm–Nd ages of the Niquelandia Layered Complex: Meso (1,25 Ga) and Neoproterozoic (0,79 Ga) extensional events in Central Brasil. Precambrian Research 132, 132-135.

Pimentel, M.M., Ferreira Filho, C.F., Armele, A., 2006. Neoproterozoic age of the Niquelândia complex, Central Brazil: further ID-TIMS and Sm–Nd isotopic evidence. Journal of South American Earth Sciences 21, 228-238.

Polat, A., Frei, R., Scherstén, A., Appel, P.W.U., 2010. New age (ca. 2970 Ma), mantle source composition and geodynamic constraints on the Archean Fiskenæsset anorthosite complex, SW Greenland. Chemical Geology 277, 1-20.

Ponce, A.D., Bertotto, G.W., Zanetti, A., Brunelli, D., Giovanardi, T., Aragón, E., Bernardi, M.I., Hémond, C., Mazzucchelli, M., 2015. Short-scale variability of the SCLM beneath the extra-Andean back-arc (Paso de Indios, Argentina): Evidence from spinel-facies mantle xenoliths. Open Geosciences 7, 362-385.

Quick, J.E., Sinigoi, S., Peressini, G., Demarchi, G.,Wooden, J.L., Sbisa, A., 2009. Magmatic plumbing of a large Permian caldera exposed to a depth of 25 km. Geology 37, 603-606.

Rivalenti, G., Correia, C.T., Girardi, V.A.V., Mazzuchelli, M., Tassinari, C.C., Bertotto, G.W., 2008. Sr–Nd isotopic evidence for crustal contamination in the Niquelandia complex, Goiàs, Central Brasil. Journal of South American Earth Sciences 25, 298-312.

Schmitz, M.D., Bowring, S.A., Ireland, T.R., 2003. Evaluation of Duluth Complex anorthositic series (AS3) zircon as a U-Pb geochronological standard: New high-precision isotope dilution thermal ionization mass spectrometry results. Geochimica et Cosmochimica Acta 67(19), 3665-3672.

Scoates, J.S., Chamberlain, K.R., 1995. Baddeleyite (ZrO2) and zircon (ZrSiO4) from anorthositic rocks of the Laramie anorthosite complex, Wyoming: Petrologic consequences and U-Pb age. American Mineralogist 80, 1317-1327.

Sforna, M.C., Lugli, F., 2017. MapIT!: a simple and user-friendly MATLAB script to elaborate elemental distribution images from LA-ICP-MS data. Journal of Analytical Atomic Spectrometry 32, 1035-1043.

Sinigoi, S., Quick, J.E., Demarchi, G., Klotzli, U., 2011. The role of crustal fertility in the generation of large silicic magmatic systems triggered by intrusion of mantle magma in the deep crust. Contributions to Mineralogy and Petrology 162, 691-707.

Trail, D., Watson, E.B., Tailby, N.D., 2012. Ce and Eu anomalies in zircon as proxies for the oxidation state of magmas. Geochimica et Cosmochimica Acta, 97, 70-87.

Vervoort, J.D., Kemp, A.I.S., 2016. Clarifyng the zircon Hf isotope record of crust-mantle evolution. Chemical Geology, 425, 65-75.

Vroon, P.Z., van der Wagt, B., Koornneef, J.M., Davies, G.R., 2008. Problems in obtaining precise and accurate Sr isotope analysis from geological materials using laser ablationMC-ICPMS. Analytical and Bioanalytical Chemistry 390, 465-476.

Williams, I.S., 1998. U-Th-Pb geochronology by ion microprobe. In: McKibben, M.A., Shanks, W.C.P., Ridley, W.I. (Eds.), Applications of Microanalytical Techniques to Understanding Mineralizing Processes, Reviews in Economic Geology 7, 1-35.

Wu, F.-Y., Yang, Y.-H., Xie, L.-W., Yang, J.-H., Xu, P., 2006. Hf isotopic compositions of standard zircons and baddeleyites used in U-Pb geochronology. Chemical Geology 234, 105-126.

Yang, W.-B., Niu, H.-C., Shan, Q., Sun, W.-D., Zhang, H., Li, N.-B., Jiang, Y.-H., Yu, X.-Y., 2014. Geochemistry of magmatic and hydrothermal zircon from the highly evolved Baerzhe alkaline granite: implications for Zr–REE–Nb mineralization. Mineralium Deposita 49, 451-470.

Figure captions

Fig. 1: regional geotectonic setting of the Goiás Massif in the Brasilia Belt modified after Oliveira Cordeiro and Oliveira (2017). Dashed-lined black boxes report the location of the three fragments of the TGSC and related detailed geological map figures in this work.

Fig. 2: geological map of the Cana Brava Complex, modified after Correia et al. (1997) and Giovanardi et al. (2017b).

Fig. 3: geological map of the Niquelândia Complex, modified after Correia et al. (2012) and Giovanardi et al. (2017b).

Fig. 4: geological map of the Barro Alto Complex, modified after Ferreira Filho et al. (2010) and Giovanardi et al. (2017b).

Fig. 5: $^{87}Sr/^{86}Sr$ and εNd recalculated at 790 Ma along the stratigraphy of the TGSC. Literature data from Niquelandia (in black) and Cana Brava (in white) are from Correia et al. (1997, 2012) and Giovanardi et al. (2017a). The Barro Alto data from this work are colored (i.e. samples BA06T, BA02T and BA01T).

Fig. 6: CL images of zircon grains from different samples of the TGSC. A) LS zircon grains showing magmatic linear zoning and domains; B) reabsorpted inherited cores in LS zircon grains with magmatic overgrowth; C) fractured and CL homogeneous zircon grains from US "Group 1"; D) anhedral to sub-euhedral zircon grains with poor zonations but distinct cores and rims from US "Group 2"; E) fragments of crystals with linear zoning and domains from "Group 3" in the US anorthosite NQ1551 of Niquelandia.

Fig. 7: CL images of zircon grains from UGAZ Barro Alto anorthosite sample BA1541 reported with the number of the SHRIMP single spot analysis; calculated concordia and average $^{206}Pb/^{238}U$ age (errors are calculated as 2σ).

Fig. 8: CL images of zircon grains from MZ Niquelandia gabbro sample NQ1549 reported with the number of the SHRIMP single spot analysis; calculated concordia and average $^{206}Pb/^{238}U$ age (errors are calculated as 2σ).

Fig. 9: CL images of zircon grains from UGAZ Niquelandia anorthosite sample NQ1552 reported with the number of the SHRIMP single spot analysis; probability density plot of $^{206}Pb/^{238}U$ age.

Fig. 10: recalculated εHf(t) for zircon grains with measured $^{206}Pb/^{238}U$ ages. (1) literature data from Della Giustina et al. (2011) from Barro Alto (BA). White-filled symbols are from LS samples while black symbols are from US samples. The Depleted Mantle (DM) evolution line is calculated using the values of present-day $^{176}Hf/^{177}Hf$ ratio of 0.28325 from Nowell et al. (1998) and $^{176}Lu/^{177}Hf$ ratio of 0.0384 from Griffin et al. (2000). CHUR values are from Blichert-Toft and Albarede (1997).

Fig. 11: zircons REE patterns normalized to the Chondrite I composition (CI; Anders and Edibara 1992). In each panel, the minimum and maximum $^{206}Pb/^{238}U$ ages in Ma obtained with LA-ICP-MS are reported.

Fig. 12: probability density plot of $^{206}Pb/^{238}U$ ages distribution for the SHRIMP zircon analyses for the LS and US of the TGSC. Reported ages are from this work and literature analyses from Correia et al. (2007; 2012), Della Giustina et al. (2011), Giovanardi et al. (2015; 2017b) and Pimentel et al. (2004).

Fig. 13: recalculated εHf(t) for zircon grains with measured U-Pb ages. (1) literature data from Della Giustina et al. (2011) from Barro Alto (BA). The Depleted Mantle (DM) evolution line is calculated using the values of present-day $^{176}Hf/^{177}Hf$ ratio of 0.28325 from Nowell et al. (1998) and $^{176}Lu/^{177}Hf$ ratio of 0.0384 from Griffin et al. (2000). CHUR values are from Blichert-Toft and Albarede (1997). US and LS inherited fields are the recalculated εHf of inherited zircons at 1.3Ga (from 5.5 to 13.9 and from -14.1 to 7.6 respectively).US and LS crust are the extimated evolutions through time of εHf from inherited bulk rock contaminants calculated from average $^{176}Hf/^{177}Hf$ initial ratio from inherited zircons and $^{176}Lu/^{177}Hf$ ratio of minimum, maximum and average ratios of bulk-rock analysis of xenoliths from LS ($^{176}Lu/^{177}Hf$ min = 0.0003, max = 0.033 and avg = 0.011; recalculated data using the 0.1419 constant of conversion from Blichert-Toft et al., 1998; Correia et al., 2012) and amphibolites ($^{176}Lu/^{177}Hf$ min = 0.009, max = 0.044 and avg = 0.023; Moraes et al., 2003).

Table captions

Table 1: sample coordinates and references for previously published U-Pb data.

Table 2: solution and in situ Sr isotope ratios from plagioclases from Barro Alto.

Table 1

Sample	Complex	Sequence	Longitude	Latitude	Lithology	Reference
CB1030	Cana Brava	LS	48°15'21.99"W	13°22'9.49"S	Diorite	Giovanardi et al. 2015, 2017b
CB1100	Cana Brava	LS	48°18'38.12"W	13°29'10.48"S	Gabbro	Giovanardi et al. 2015, 2017b
CB1175	Cana Brava	LS	48°16'3.61"W	13°28'0.01"S	Gabbro	Giovanardi et al. 2015, 2017b
CB1382	Cana Brava	LS	48°15'32.05"W	13°22'6.06"S	Gabbro	Giovanardi et al. 2015, 2017b
NQ1549	Niquelandia	LS	48°29'56.40"W	14°21'49.59"S	Gabbro	This work
NQ1551	Niquelandia	US	48°31′39.40″W	14°22′4.59″S	Anorthosite	Correia et al. 2012
NQ1552	Niquelandia	US	48°31’58”W	14°22’01”S	Anorthosite	Correia et al. 2007
BA06T	Barro Alto	LS	49°11'23.94"W	15°12'51.04"S	Gabbro	Giovanardi et al. 2017b
BA01T	Barro Alto	US	48°59'17.91"W	15°05'02.13"S	Anorthosite	Giovanardi et al. 2017b
BA1541	Barro Alto	US	49°02’25”W	15°05’17”S	Anorthosite	Correia et al. 2007

Table 2: Sr isotopes from Barro Alto samples

Sample	**Unit**	**$^{87}Sr/^{86}Sr$**	**2σ**	**Rb/Sr**	**$^{87}Sr/^{86}Sr_{(790)}$**
solution					
BA02T	UGAZ	0.702368	0.000012	0.0020	0.702355
BA06T	MZ	0.729226	0.000012	0.0030	0.729192
in situ					
BA01T	UGAZ	0.702452	0.000040	0.0011	0.702430
BA02T	UGAZ	0.702444	0.000329	0.0020	0.702432
BA06T	MZ	0.729948	0.000125	0.0030	0.729914

Highlights

Zircon and plagioclase geochronological and geochemical study of the contamination of the Tonian Goias Stratiform Complex

$^{176}Hf/^{177}Hf$ and $^{87}Sr/^{86}Sr$ ratios in zircon and plagioclase reveal a crustal contamination for the Lower Sequence and a mantle-derived contamination for the Upper Sequence

The geochemical affinity of the country rock controls the differential contamination history of the TGSC Lower and Upper Sequences

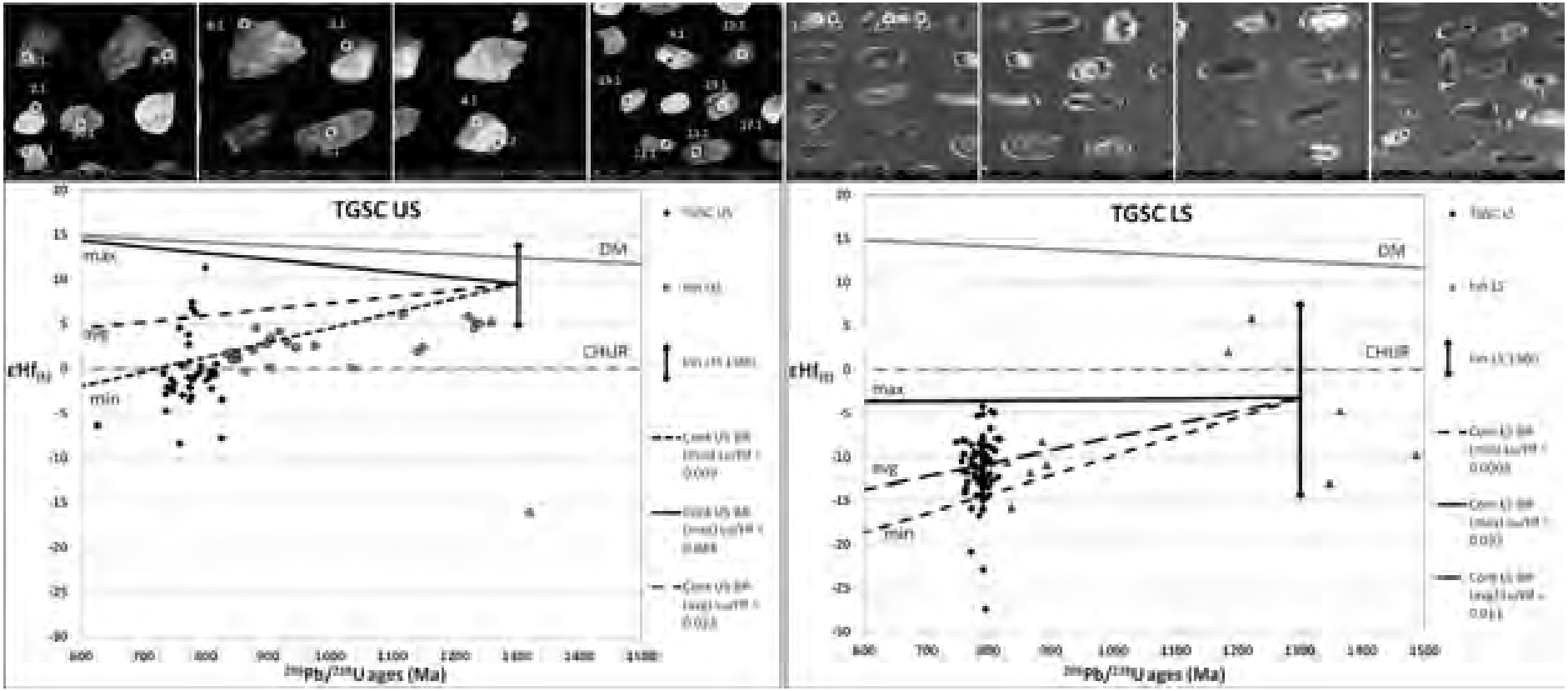

Graphics Abstract

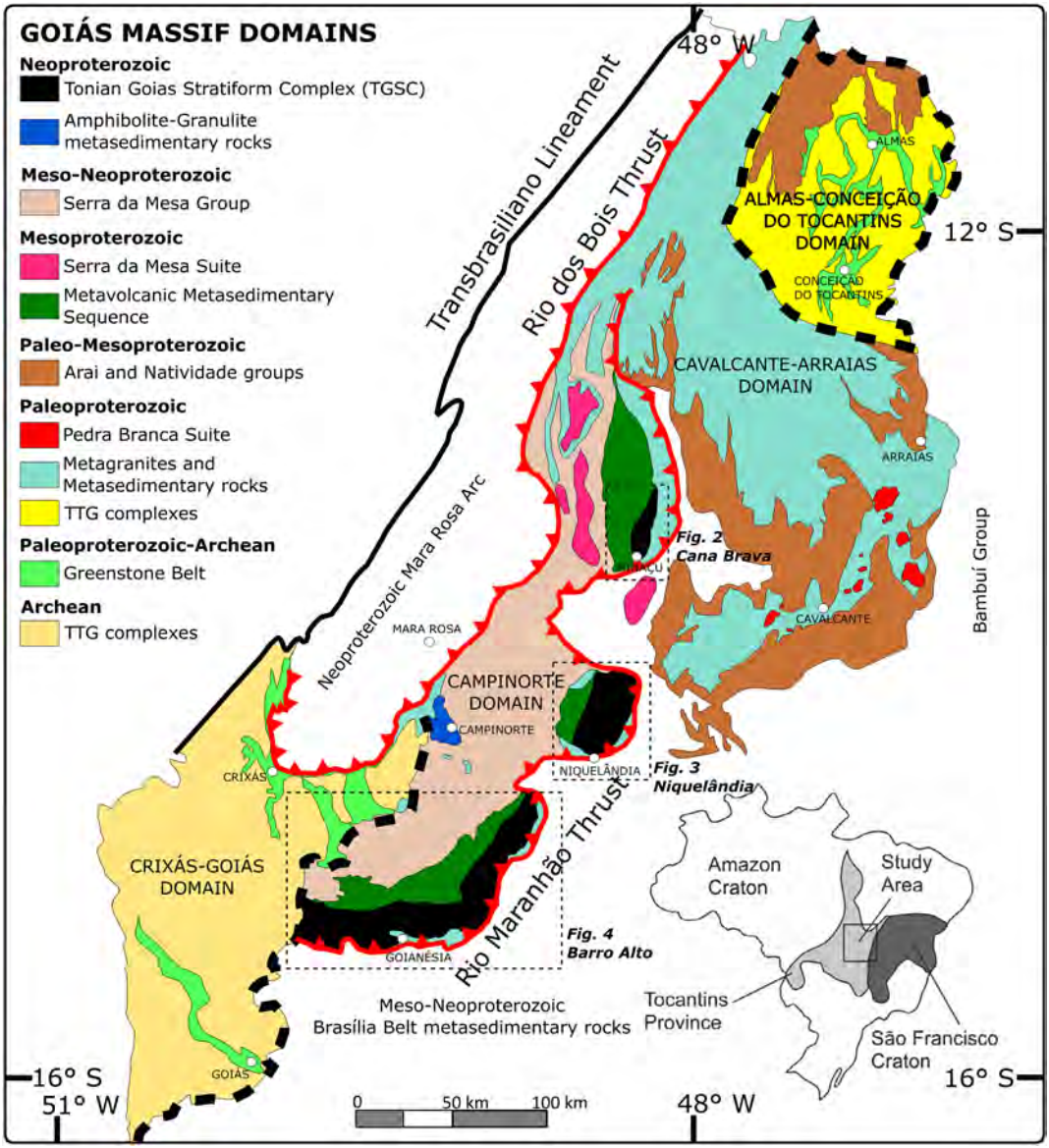
GOIÁS MASSIF DOMAINS
Neoproterozoic
Tonian Goias Stratiform Complex (TGSC)
Amphibolite-Granulite metasedimentary rocks
Meso-Neoproterozoic
Serra da Mesa Group
Mesoproterozoic
Serra da Mesa Suite
Metavolcanic Metasedimentary Sequence
Paleo-Mesoproterozoic
Arai and Natividade groups
Paleoproterozoic
Pedra Branca Suite
Metagranites and Metasedimentary rocks
TTG complexes
Paleoproterozoic-Archean
Greenstone Belt
Archean
TTG complexes
Transbrasiliano Lineament
Rio dos Bois Thrust
Neoproterozoic Mara Rosa Arc
Rio Maranhão Thrust
48° W
12° S
16° S
51° W
ALMAS-CONCEIÇÃO DO TOCANTINS DOMAIN
ALMAS
CONCEIÇÃO DO TOCANTINS
CAVALCANTE-ARRAIAS DOMAIN
ARRAIAS
CAVALCANTE
Bambuí Group
Fig. 2 Cana Brava
MARA ROSA
CAMPINORTE DOMAIN
CAMPINORTE
NIQUELÂNDIA
Fig. 3 Niquelândia
CRIXÁS
CRIXÁS-GOIÁS DOMAIN
GOIANÉSIA
Fig. 4 Barro Alto
GOIÁS
Meso-Neoproterozoic Brasília Belt metasedimentary rocks
Amazon Craton
Study Area
Tocantins Province
São Francisco Craton
0
50 km
100 km

Figure 1

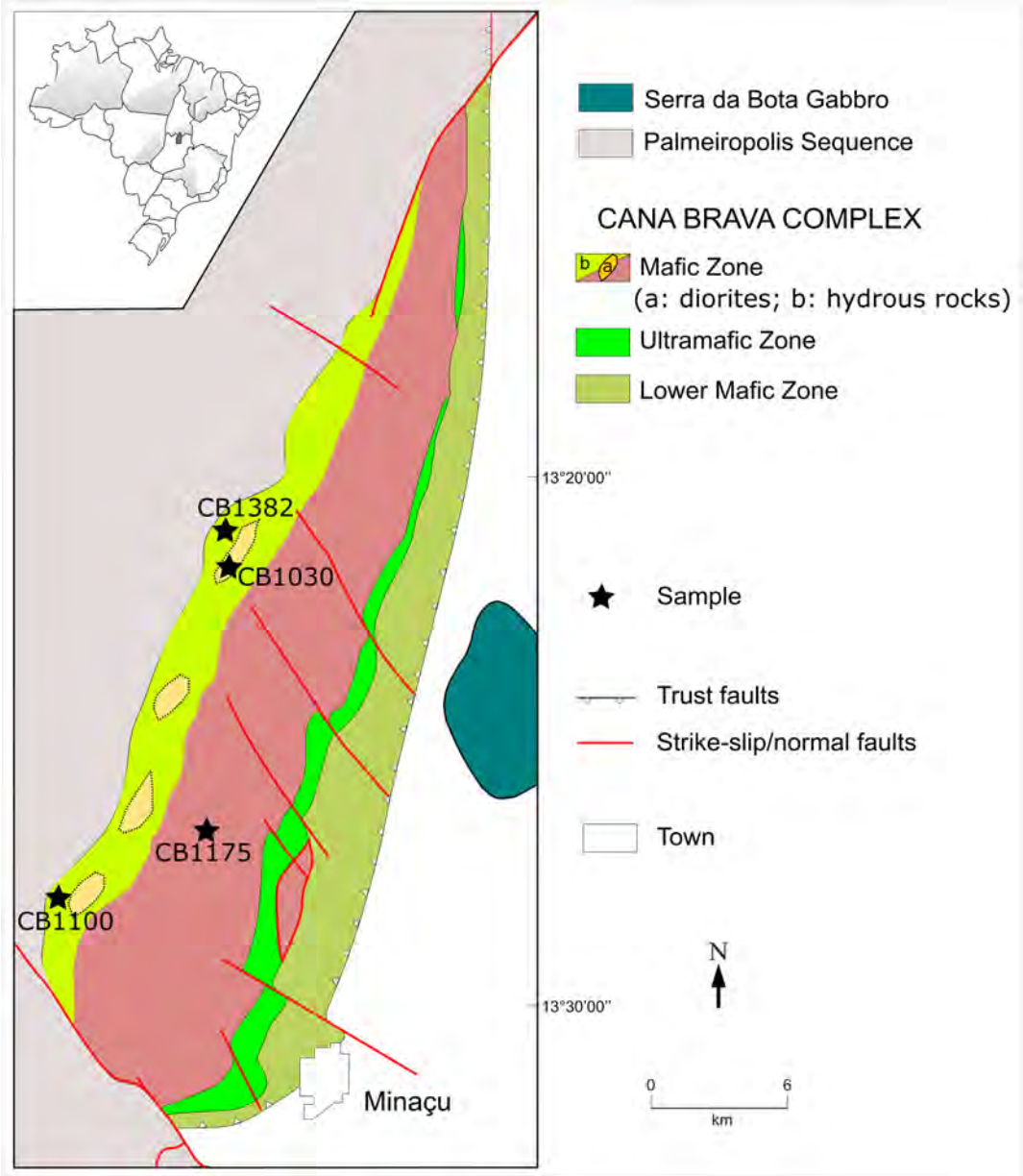
Serra da Bota Gabbro
Palmeiropolis Sequence
CANA BRAVA COMPLEX
b a
Mafic Zone
(a: diorites; b: hydrous rocks)
Ultramafic Zone
Lower Mafic Zone
13°20'00"
CB1382
CB1030
Sample
Trust faults
Strike-slip/normal faults
Town
CB1175
CB1100
N
13°30'00"
Minaçu
0
6
km

Figure 2

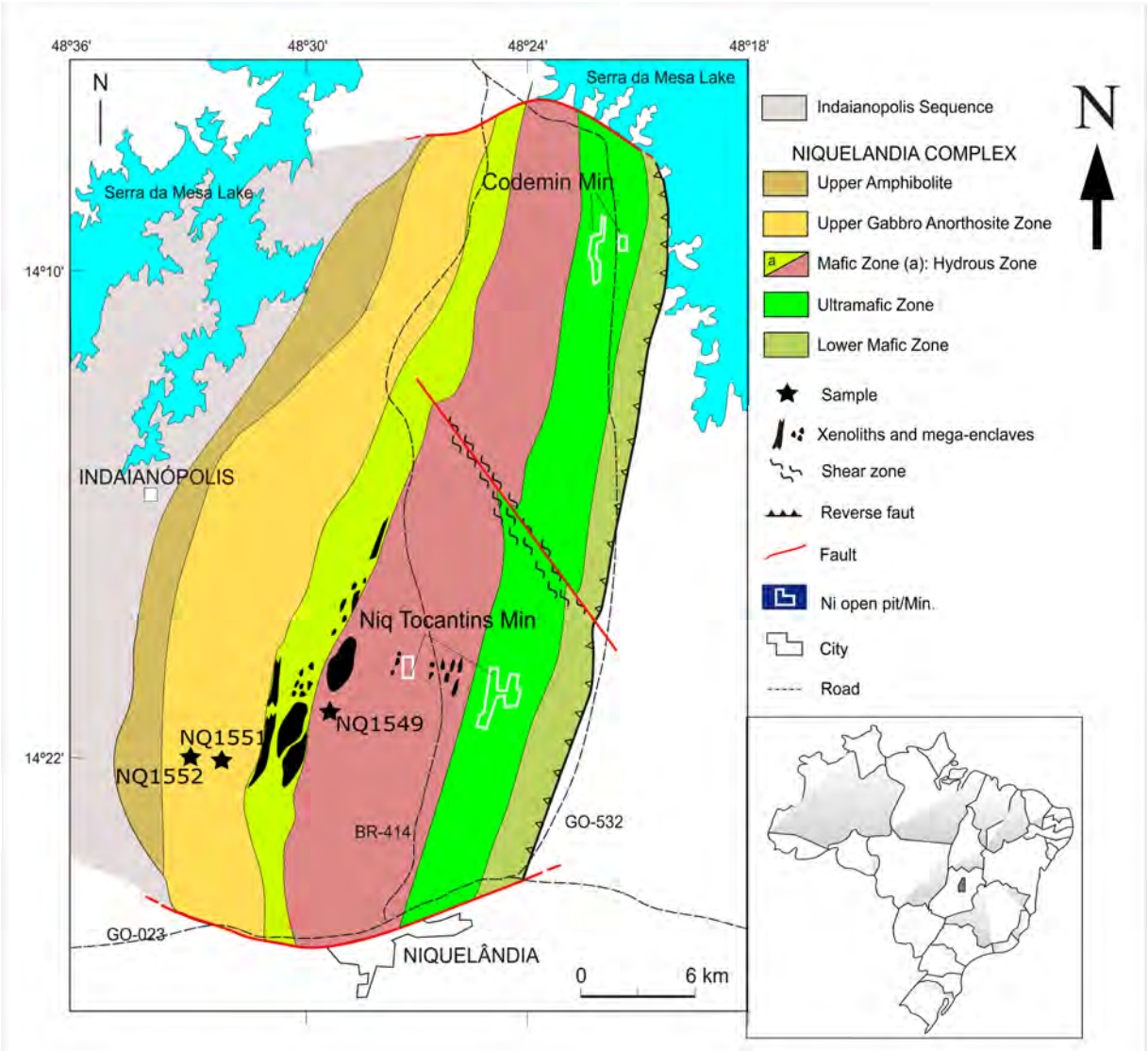
48°36'
48°30'
48°24'
48°18'
14°10'
14°22'
N
Serra da Mesa Lake
Serra da Mesa Lake
Codemin Min
INDAIANÓPOLIS
Niq Tocantins Min
NQ1549
NQ1551
NQ1552
BR-414
GO-532
GO-023
NIQUELÂNDIA
0
6 km
Indaianopolis Sequence
NIQUELANDIA COMPLEX
Upper Amphibolite
Upper Gabbro Anorthosite Zone
Mafic Zone (a): Hydrous Zone
Ultramafic Zone
Lower Mafic Zone
Sample
Xenoliths and mega-enclaves
Shear zone
Reverse faut
Fault
Ni open pit/Min.
City
Road
N

Figure 3

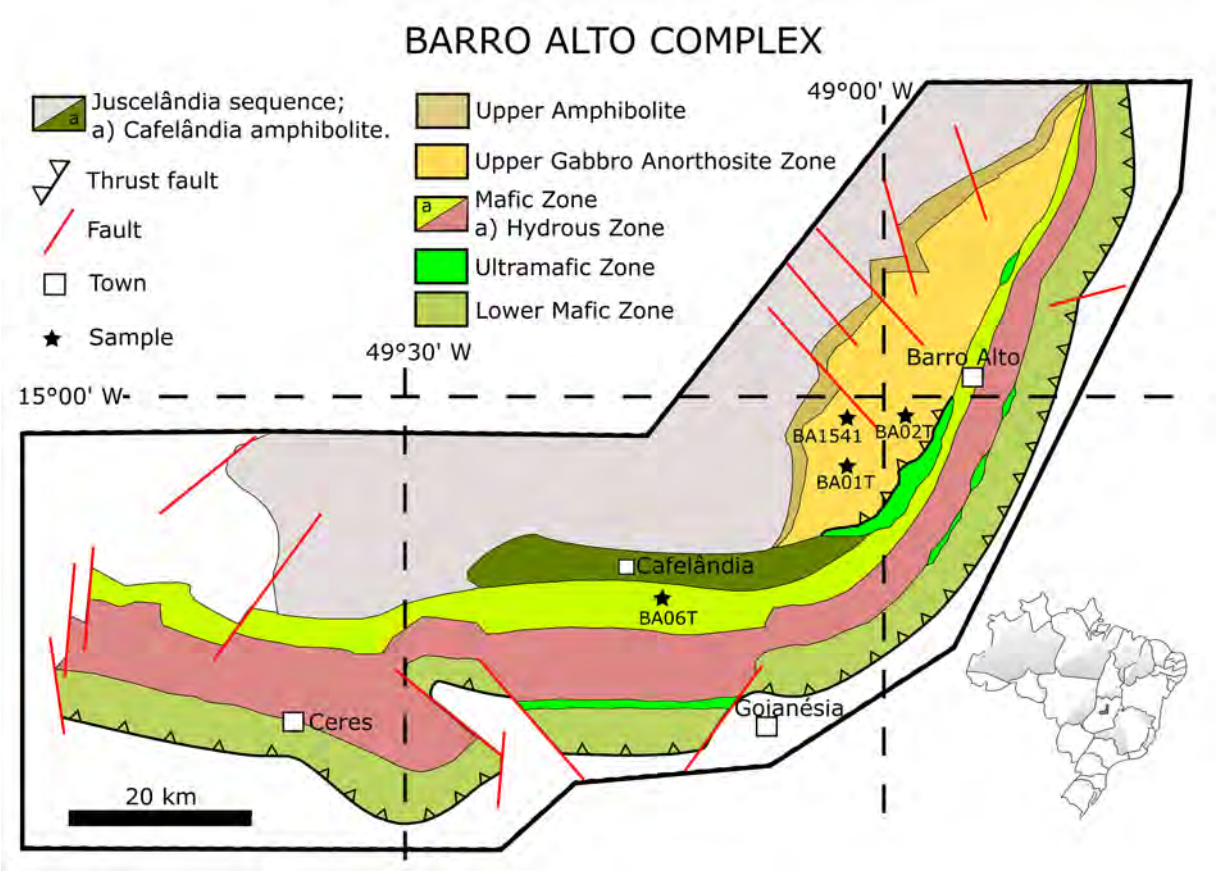
BARRO ALTO COMPLEX
Juscelândia sequence;
a) Cafelândia amphibolite.
Thrust fault
Fault
Town
Sample
Upper Amphibolite
Upper Gabbro Anorthosite Zone
Mafic Zone
a) Hydrous Zone
Ultramafic Zone
Lower Mafic Zone
49°00' W
49°30' W
15°00' W
Barro Alto
BA1541
BA02T
BA01T
Cafelândia
BA06T
Ceres
Goianésia
20 km

Figure 4

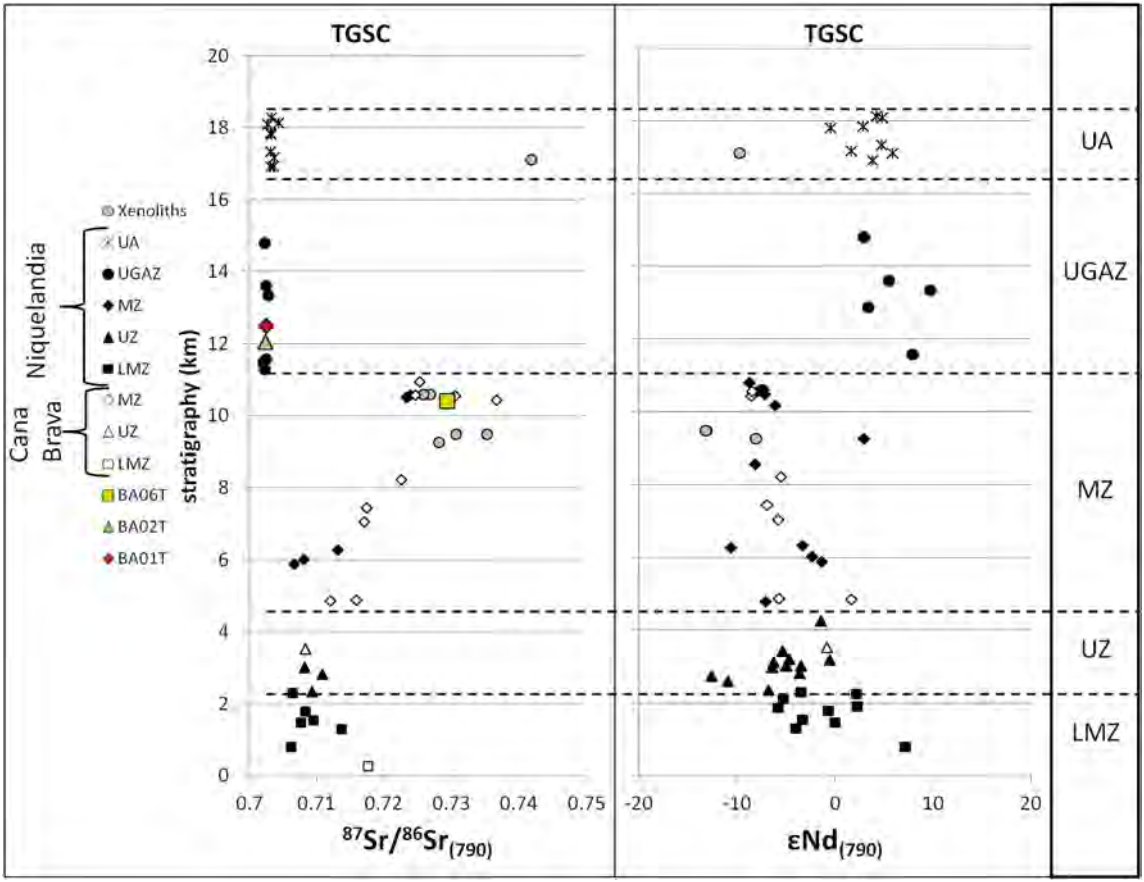
TGSC
TGSC
Xenoliths
UA
UGAZ
MZ
UZ
LMZ
Niquelandia
MZ
UZ
LMZ
Cana Brava
BA06T
BA02T
BA01T
stratigraphy (km)
0
2
4
6
8
10
12
14
16
18
20
0.7
0.71
0.72
0.73
0.74
0.75
$^{87}Sr/^{86}Sr_{(790)}$
-20
-10
0
10
20
$\varepsilon Nd_{(790)}$
UA
UGAZ
MZ
UZ
LMZ

Figure 5

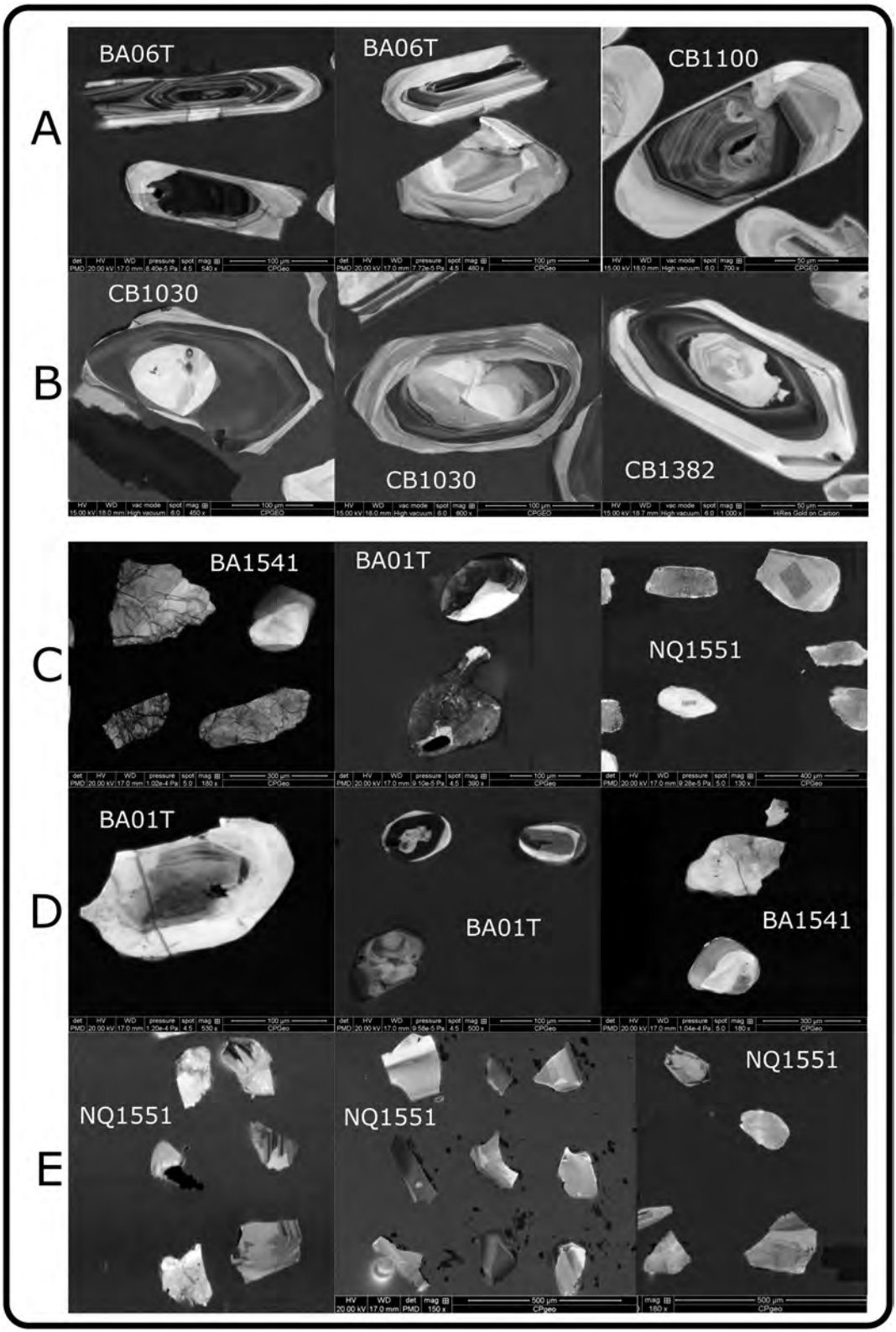
A
BA06T
BA06T
CB1100
B
CB1030
CB1030
CB1382
C
BA1541
BA01T
NQ1551
D
BA01T
BA01T
BA1541
E
NQ1551
NQ1551
NQ1551

Figure 6

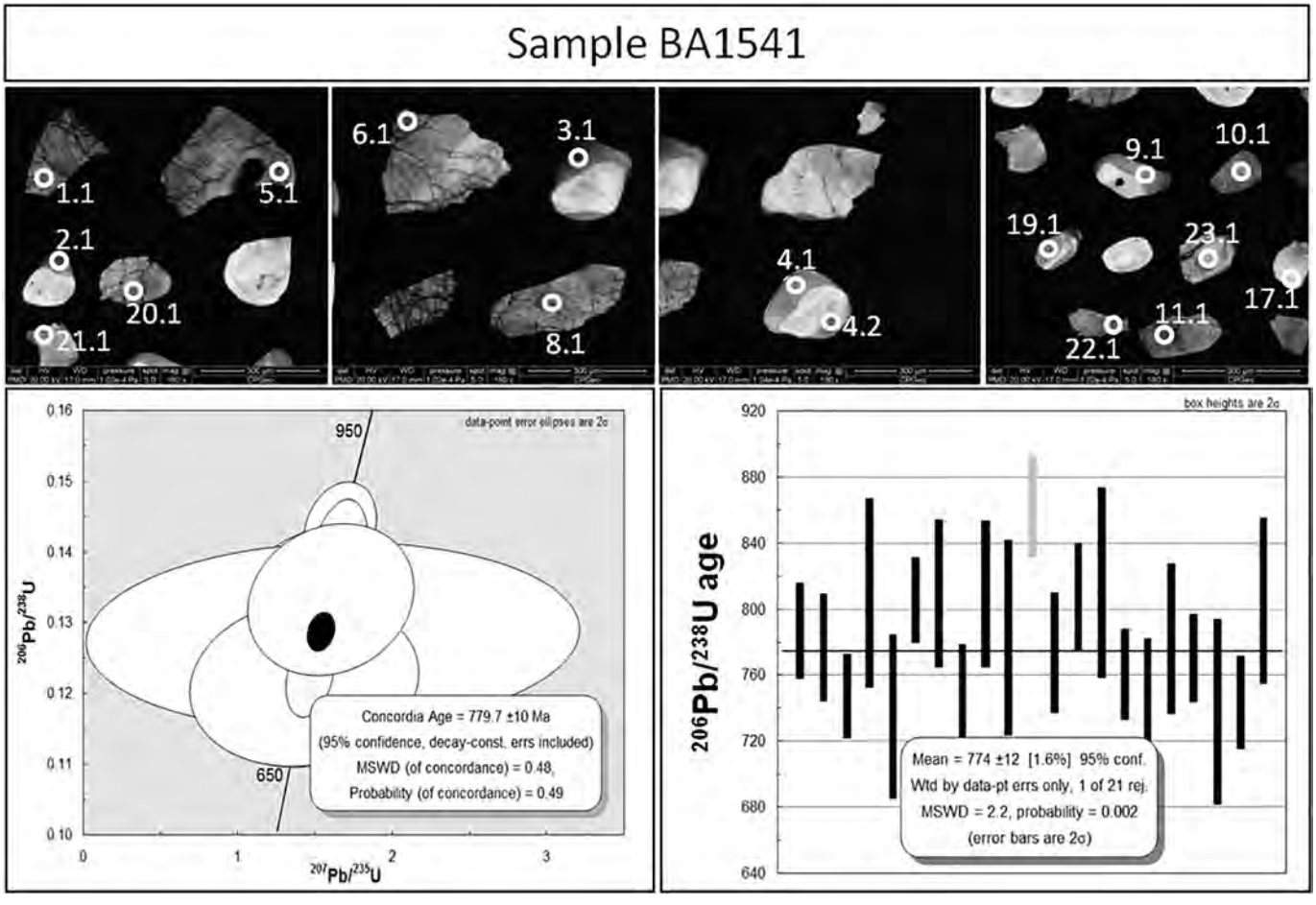
Sample BA1541
1.1
2.1
20.1
21.1
5.1
6.1
3.1
8.1
4.1
4.2
9.1
10.1
19.1
23.1
17.1
11.1
22.1
data-point error ellipses are 2σ
950
650
Concordia Age = 779.7 ±10 Ma
(95% confidence, decay-const. errs included)
MSWD (of concordance) = 0.48,
Probability (of concordance) = 0.49
206Pb/238U
207Pb/235U
box heights are 2σ
206Pb/238U age
Mean = 774 ±12 [1.6%] 95% conf.
Wtd by data-pt errs only, 1 of 21 rej.
MSWD = 2.2, probability = 0.002
(error bars are 2σ)

Figure 7

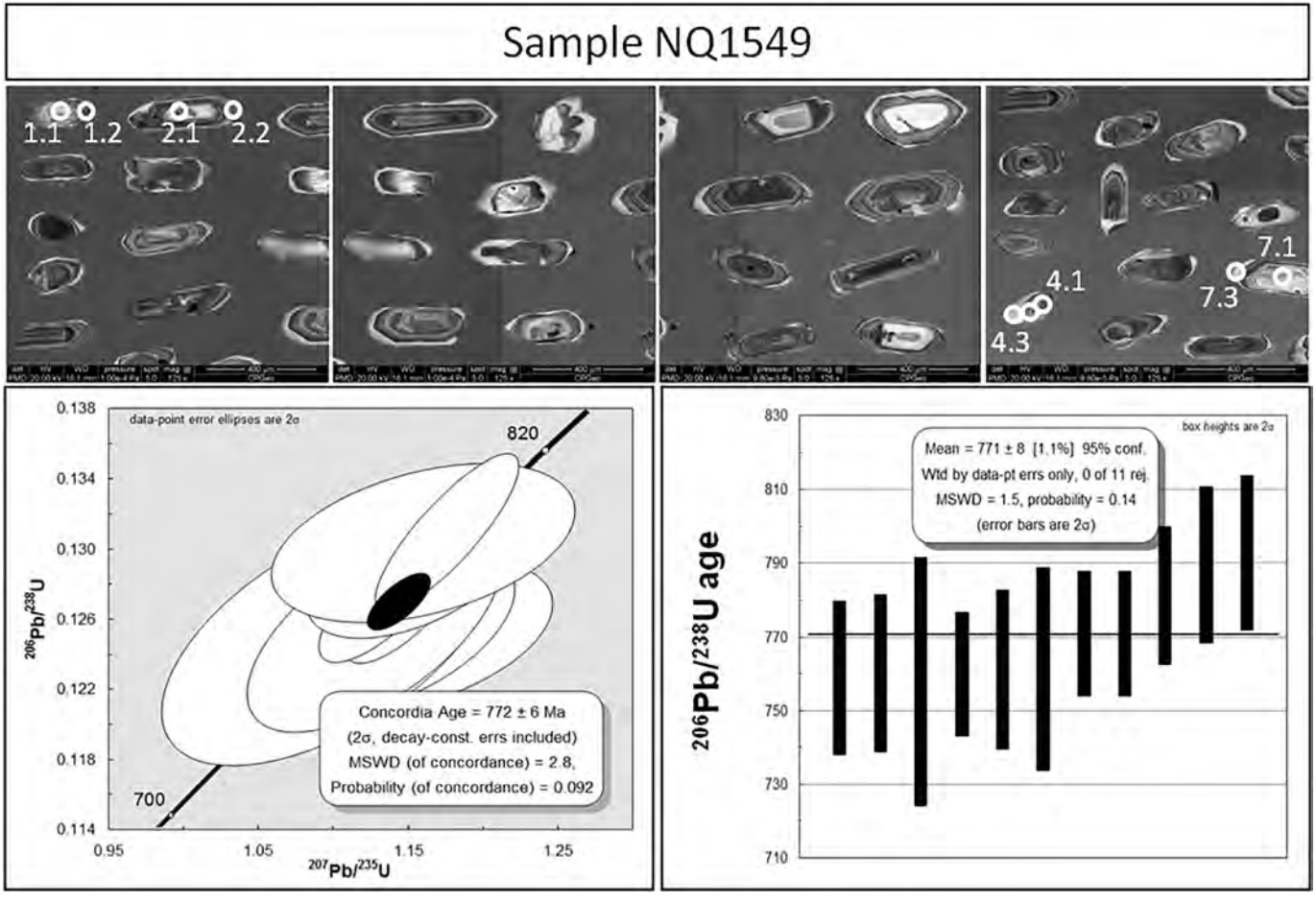
Sample NQ1549
1.1
1.2
2.1
2.2
4.1
4.3
7.1
7.3
data-point error ellipses are 2σ
820
700
Concordia Age = 772 ± 6 Ma
(2σ, decay-const. errs included)
MSWD (of concordance) = 2.8,
Probability (of concordance) = 0.092
$^{206}Pb/^{238}U$
$^{207}Pb/^{235}U$
0.138
0.134
0.130
0.126
0.122
0.118
0.114
0.95
1.05
1.15
1.25
box heights are 2σ
Mean = 771 ± 8 [1.1%] 95% conf.
Wtd by data-pt errs only, 0 of 11 rej.
MSWD = 1.5, probability = 0.14
(error bars are 2σ)
$^{206}Pb/^{238}U$ age
830
810
790
770
750
730
710

Figure 8

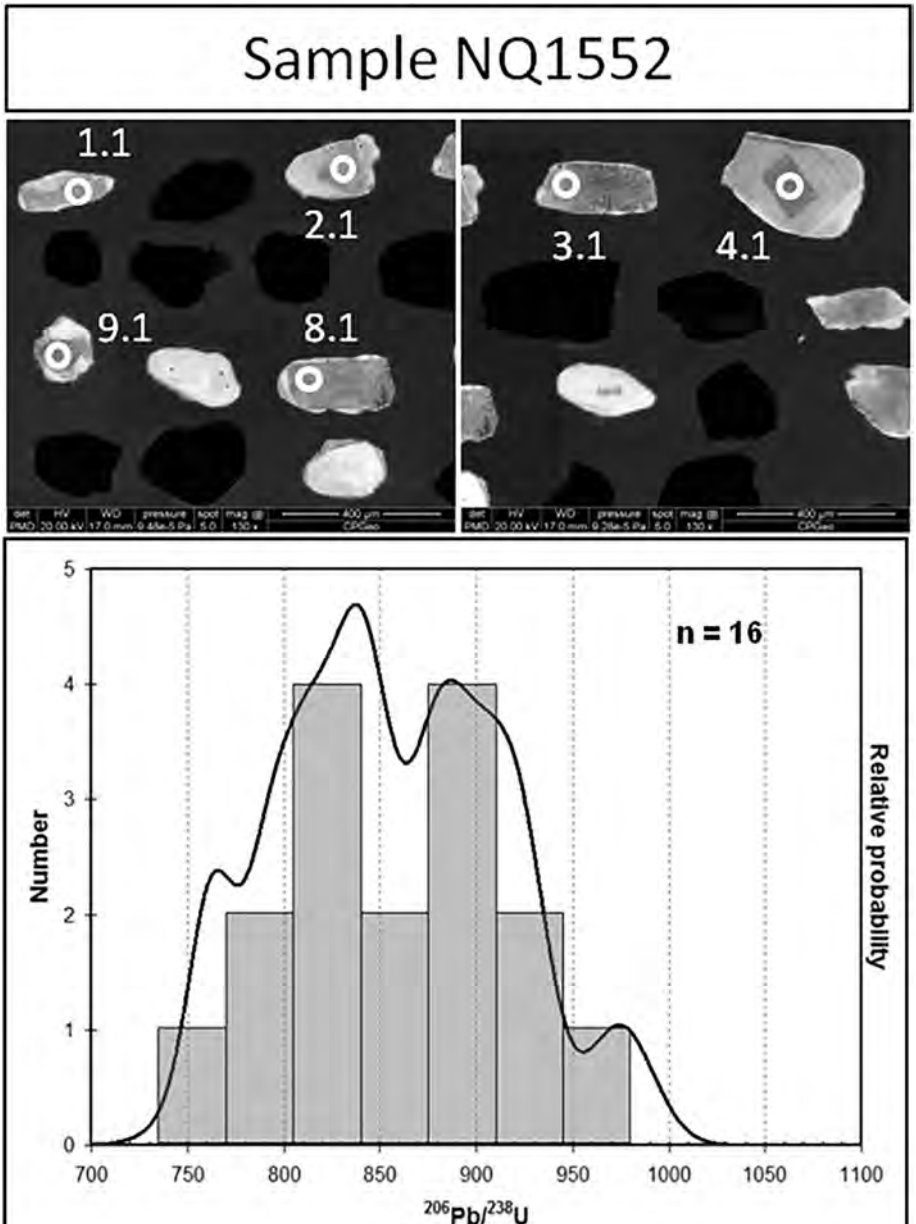
Sample NQ1552
1.1
2.1
9.1
8.1
3.1
4.1
n = 16
Number
Relative probability
0
1
2
3
4
5
700
750
800
850
900
950
1000
1050
1100
$^{206}Pb/^{238}U$

Figure 9

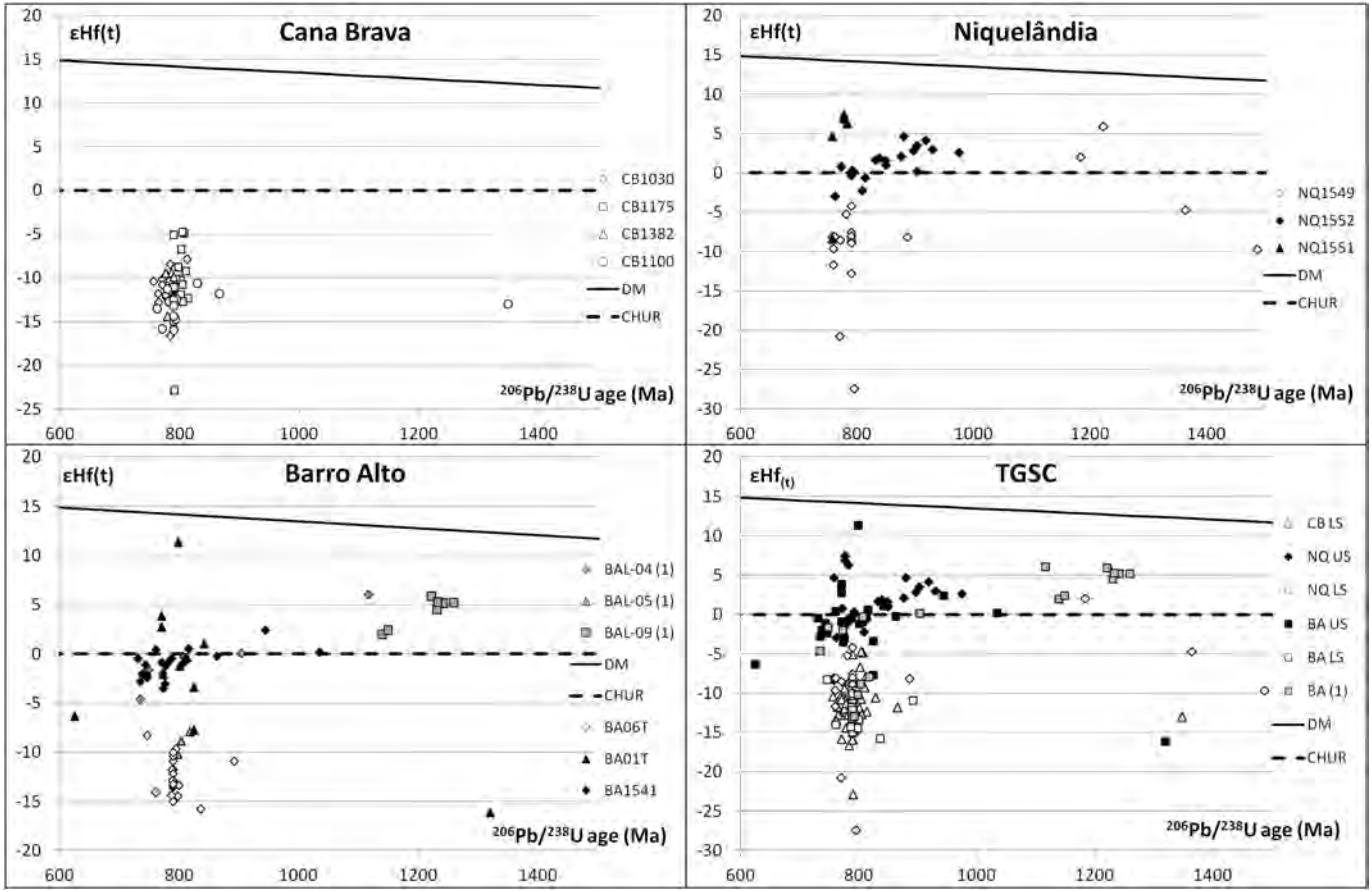
εHf(t)
Cana Brava
CB1030
CB1175
CB1382
CB1100
DM
CHUR
206Pb/238U age (Ma)
εHf(t)
Niquelândia
NQ1549
NQ1552
NQ1551
DM
CHUR
206Pb/238U age (Ma)
εHf(t)
Barro Alto
BAL-04 (1)
BAL-05 (1)
BAL-09 (1)
DM
CHUR
BA06T
BA01T
BA1541
206Pb/238U age (Ma)
εHf(t)
TGSC
CB LS
NQ US
NQ LS
BA US
BA LS
BA (1)
DM
CHUR
206Pb/238U age (Ma)

Figure 10

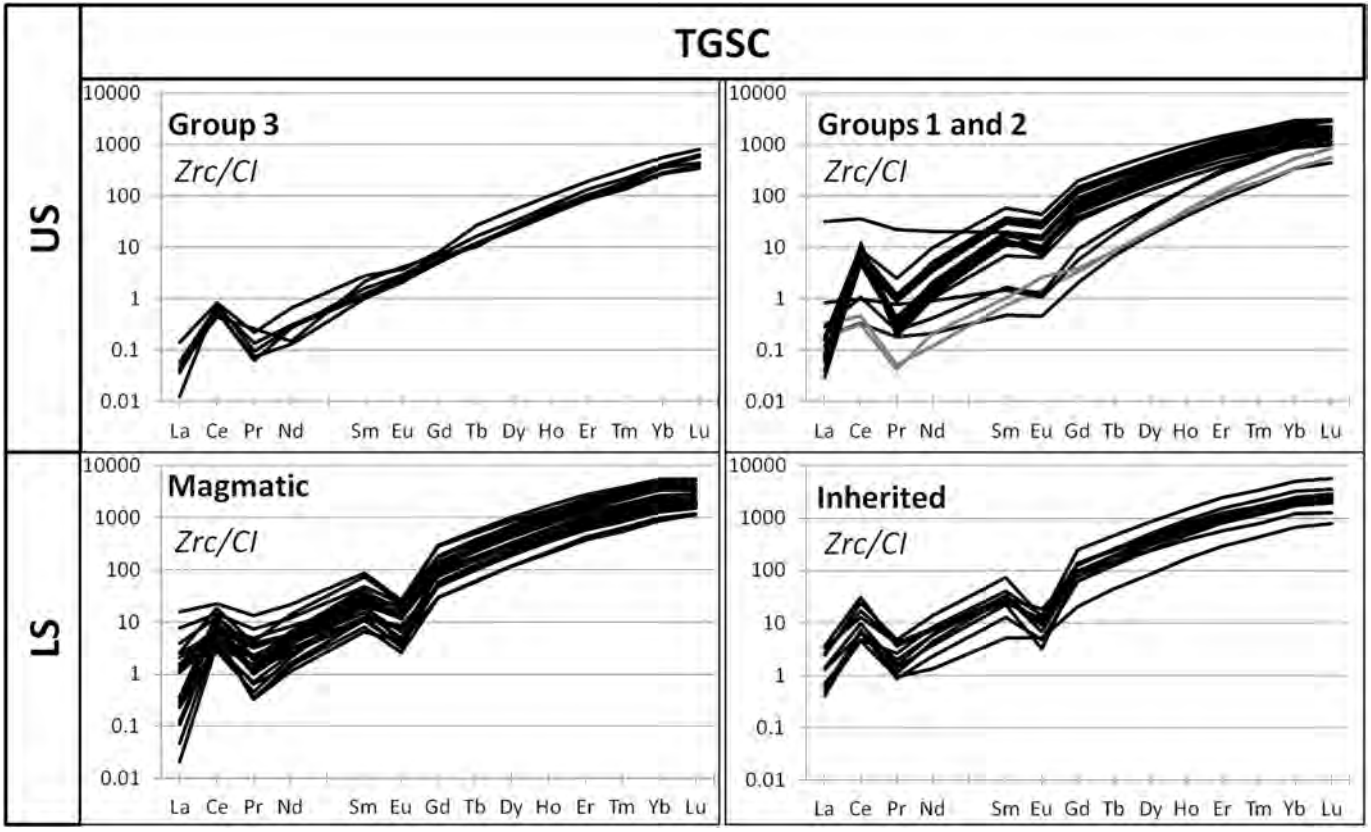
TGSC
US
LS
Group 3
Zrc/Cl
Groups 1 and 2
Zrc/Cl
Magmatic
Zrc/Cl
Inherited
Zrc/Cl
10000
1000
100
10
1
0.1
0.01
La Ce Pr Nd Sm Eu Gd Tb Dy Ho Er Tm Yb Lu

Figure 11

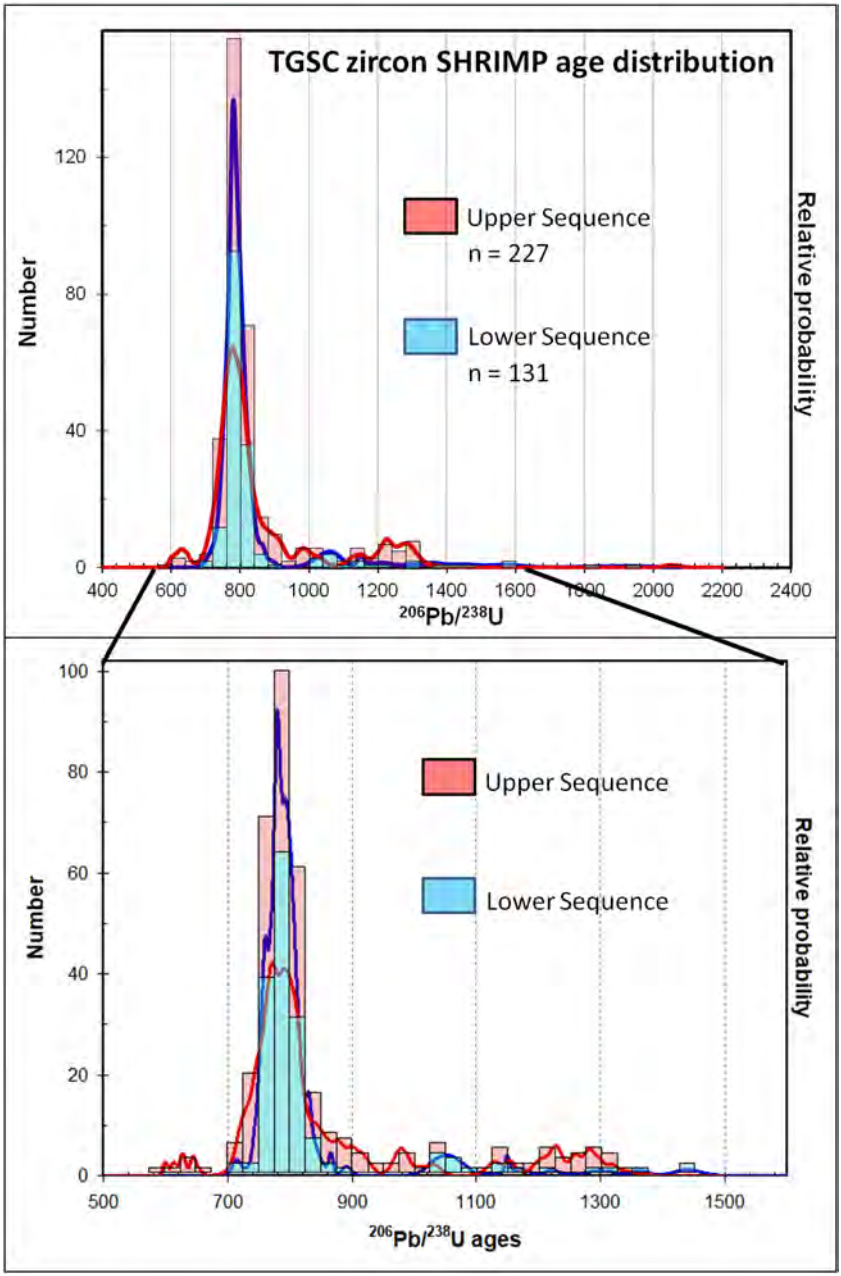
TGSC zircon SHRIMP age distribution
Upper Sequence
n = 227
Lower Sequence
n = 131
Number
Relative probability
206Pb/238U
Upper Sequence
Lower Sequence
Number
Relative probability
206Pb/238U ages

Figure 12

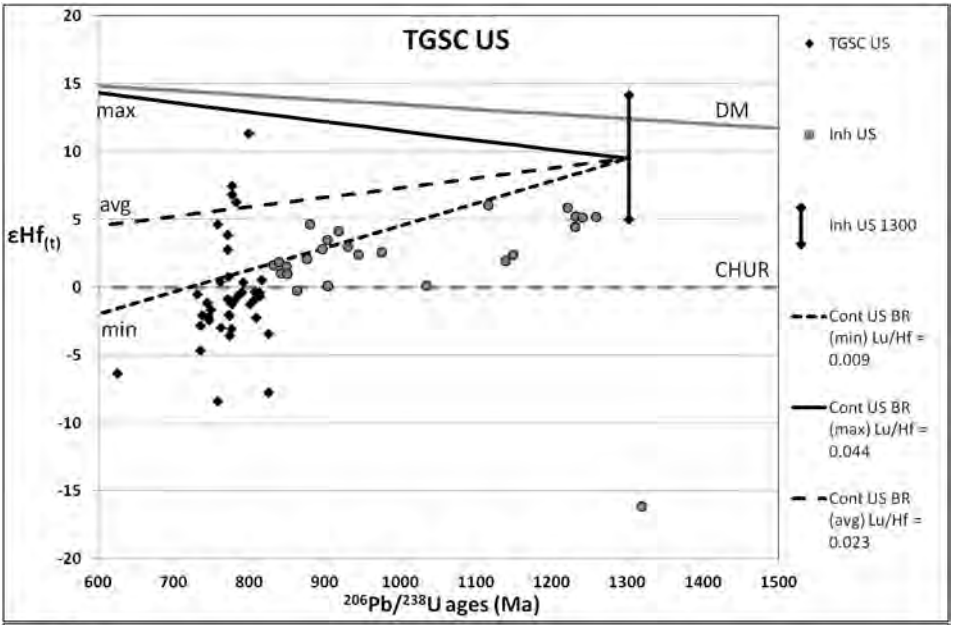
TGSC US
εHf(t)
206Pb/238U ages (Ma)
max
avg
min
DM
CHUR
TGSC US
Inh US
Inh US 1300
Cont US BR (min) Lu/Hf = 0.009
Cont US BR (max) Lu/Hf = 0.044
Cont US BR (avg) Lu/Hf = 0.023

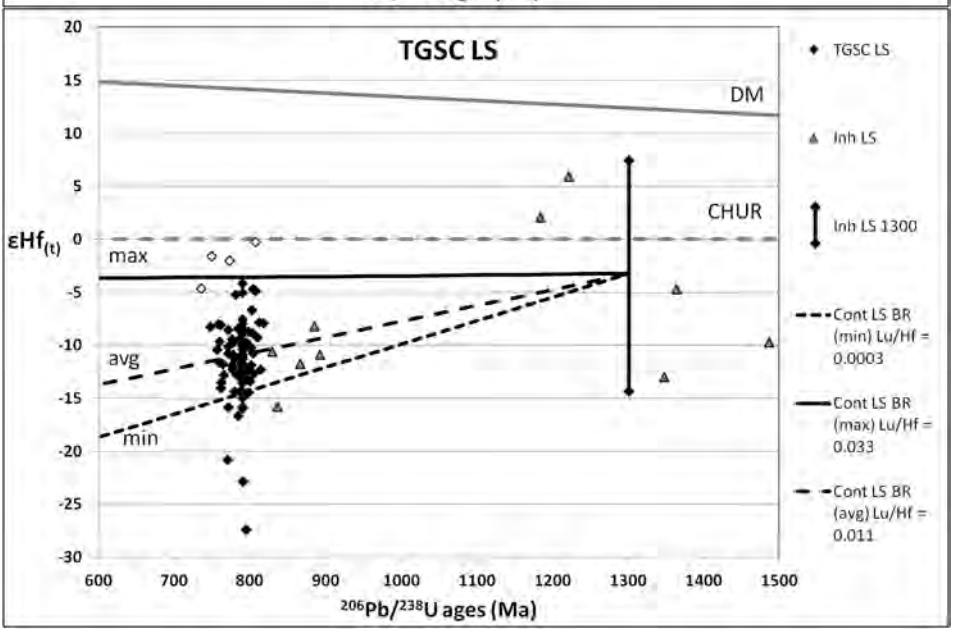
TGSC LS
εHf(t)
206Pb/238U ages (Ma)
max
avg
min
DM
CHUR
TGSC LS
Inh LS
Inh LS 1300
Cont LS BR (min) Lu/Hf = 0.0003
Cont LS BR (max) Lu/Hf = 0.033
Cont LS BR (avg) Lu/Hf = 0.011

Figure 13